Recent Particle Formation and Aerosol Variability Near Southern Ocean Low Clouds

Isabel L. McCoy[1], Christopher S. Bretherton[1], Robert Wood[1], Cynthia H. Twohy[2], Andrew Gettelman[3], Charles G. Bardeen[3], and Darin W. Toohey[4]

[1] Atmospheric Sciences, University of Washington, Seattle, WA, USA, [2] Northwest Research Associates, Redmond, WA, USA, [3] National Center for Atmospheric Research, Boulder, CO, USA, [4]Atmospheric and Oceanic Sciences, University of Colorado, Boulder, CO, USA.

Corresponding author: Isabel L. McCoy (imccoy@uw.edu)

Key Points:

- Summertime Southern Ocean free tropospheric aerosol number is dominated by Aitken particles recently generated through synoptic uplift.
- Sub-cloud, dominantly sulfur-based cloud condensation nuclei control summertime Southern Ocean droplet number concentrations.
- Free-tropospheric Aitken aerosol buffer Southern Ocean cloud condensation nuclei and cloud droplet numbers against precipitation removal.

Abstract

Controls on the pristine aerosol population over the Southern Ocean (SO) are critical for constraining the strength of global aerosol indirect forcing. The 2018 SOCRATES aircraft campaign sampled summertime clouds and aerosols across varied SO synoptic conditions during repeated southerly transects (140-160°E, 45-62°S). The SO free troposphere (3-6 km) is characterized by frequent recent particle formation (RPF) events contributing to large (>1000 cm^{-3}) and widespread concentrations of condensation nuclei (diameters > 11 nm), consistently higher than other low cloud regions (e.g. North East Pacific). A SO synoptic uplift mechanism responsible for producing free tropospheric Aitken-mode particles (11-100 nm) is identified using SOCRATES measurements, air-mass trajectories, and reanalysis. SO cloud droplet number concentrations (N_d~100 cm^{-3}) are controlled by sub-cloud cloud condensation nuclei (CCN, 100-1000nm), but direct emissions (i.e. sea spray) are not the largest contributor to summertime CCN. Sub-micron aerosol number concentration in, above, and sub-cloud is dominated by sulfur-based particles, consistent with growth of free tropospheric Aitken particles with DMS-oxidation product volatility signatures. We propose a hypothesis for SO cloud-aerosol interactions: above-cloud Aitken mode particles grow in and sub-cloud to dominate sub-cloud summertime CCN, acting to buffer clouds and aerosols against precipitation removal and leading to persistently high summertime SO N_d. Aerosol and cloud prediction capabilities in nudged hindcasts from the Community Atmosphere Model (CAM6) are tested. CAM6 underpredicts N_d but matches observed CCN despite sea-spray dominance in the model, indicating incomplete representations of biological aerosol production mechanisms and associated summertime aerosol-cloud interactions.

Plain Language Summary

The remote Southern Ocean (SO) is a unique analog to pre-industrial environments due to limited continental or anthropogenic influences. Understanding how aerosols are produced in this region and their influence on clouds, particularly cloud brightness driven by cloud droplet number, is vital for understanding the change in sunlight reflected by clouds due to the addition of anthropogenic emissions during industrialization. This is essential for increasing accuracy of climate change projections. To understand this pristine environment, we analyze novel observations of SO clouds and aerosols from a summertime aircraft campaign. We present evidence for a new aerosol production mechanism driven by synoptic storms and sourced from emissions of ocean biology. This mechanism produces a reservoir of small aerosols above cloud that are likely the missing source of sub-cloud aerosol that grows into cloud droplets and influences SO cloud brightness. The importance of these above-cloud aerosols is clear as biological aerosol is a larger contributor to cloud droplet number than sea-spray aerosol. We propose that the above-cloud reservoir of biological aerosol is key in creating long-lasting and bright SO clouds, which has important implications for understanding pre-industrial environments and their response to anthropogenic aerosol.

1 Introduction

The Southern Ocean (SO) plays a key role in understanding our past and present climate due to the pristine nature of its aerosol, the closest analog we have to the pre-industrial state [*Hamilton et al.,* 2014]. Understanding the climate response to changes in anthropogenic aerosol

will help to reduce the uncertainty in global climate model (GCM) climate sensitivity and improve climate predictions [*Andreae et al.*, 2005; *Forster*, 2016]. Recent work has shown that forcing from aerosol-cloud interactions is the main contributor to uncertainty in total radiative forcing [*Bellouin*, 2019], and the poorly understood pre-industrial aerosol state is a leading driver [*Carslaw et al.*, 2013]. While we cannot measure pre-industrial aerosol, we *can* examine aerosol-cloud interactions in the few remaining pristine locations in the present-day in order to reduce the associated uncertainty in indirect and thus total radiative forcing.

Southern Hemisphere (SH) oceans are an ideal location for studying pre-industrial aerosol-cloud interactions as they are one of the few remaining pristine aerosol environments and are frequently cloudy [*Hamilton et al.*, 2014]. The influence of anthropogenic and biomass burning aerosol is mostly negligible over SH oceans, particularly in the summertime, leaving sea spray and biologically sourced aerosols as the primary contributors to the aerosol budget. Aerosols fall roughly into three modes: nucleation or Aitken (diameters between 0.005 and 0.1 μm), accumulation (diameters between 0.1 and 2.5 μm), and coarse (diameters > 2.5 μm) [*Seinfeld and Pandis*, 2006]. The number concentration of particles in the SO is dominated by Aitken mode and small accumulation mode particles while the mass is dominated by coarse mode particles [*Ayers et al.*, 1997]. Accumulation mode aerosols are the primary cloud condensation nuclei (CCN) and are of central importance to aerosol-cloud interactions through their control of cloud droplet number (N_d) and overall cloud albedo [*Twomey*, 1977].

In the summertime SO and other biologically active pristine marine regions, phytoplankton emissions of dimethyl sulfide (DMS) play a key role in both production of Aitken mode particles and growth of CCN [*Ayers et al.*, 1997; *Ayers and Gillett*, 2000; *Ayers and Gras*, 1991; *Charlson et al.*, 1987]. CCN grow from coagulation of smaller Aitken or accumulation mode particles; from vapor deposition onto preexisting particles [*Seinfeld and Pandis*, 2006]; and from the addition of non-sea-salt sulfate derived from aqueous-phase oxidation of DMS products in cloud droplets that subsequently evaporate, contributing to the accumulation mode budget [*Charlson et al.*, 1987; *Hobbs*, 1971].

Aitken mode particles form through homogeneous nucleation of precursor gases [*Seinfeld and Pandis*, 2006]. Two major precursor gases in the marine environment are sulfuric acid (H_2SO_4) and methane sulfonic acid (MSA), both oxidation products of DMS [*Ayers et al.*, 1997; *Fitzgerald*, 1991]. For gas to particle conversion to occur, precursor gases must be present and the total aerosol surface area (primarily from coarse and accumulation mode sized aerosols) must be low enough to discourage vapor deposition on preexisting particles (<10-20 μg cm^{-3}) [*Covert et al.*, 1996]. The latter is more likely in the free troposphere (FT) [*Clarke*, 1993]. SO observations indicate particles with diameters ≤ 0.5 μm are primarily non-sea-salt sulfate, indicating formation was assisted by DMS oxidation products [*Fitzgerald*, 1991]. Along with sulfuric acid, ions, organics, and other compounds can also play a role in particle formation [*Gordon et al.*, 2017].

Sea spray aerosol production mechanisms contribute to the upper end of the accumulation mode size range and the coarse mode [*Grythe et al.*, 2014]. In the wintertime, sea spray dominates the boundary layer aerosol signature as biogenic sources are inactive. However, most of the aerosol particles with diameters ≤ 0.2 μm are not composed of sea spray or organics in the summertime but are dominated by non-sea-salt sulfate [*Bigg*, 2007; *Bigg and Leck*, 2008; *Fossum et al.*, 2018]. From a synthesis of observations and modeling studies, entrainment of new particles from the FT is thought to be the main source of aerosol number in marine regions at low and middle latitudes [*Kerminen et al.*, 2018].

Taken together, these studies broadly suggest that the majority of Aitken mode particles in marine regions are produced through gas to particle conversion of DMS oxidation products, that these particles may be forming in the FT, and that they are likely important in controlling the summertime Southern Ocean CCN number concentrations. These three ideas are the fundamental basis for our analysis and have been the subject of many other papers.

There is evidence for new particle formation occurring aloft in the SH during austral summer associated with DMS-oxidation products. Aitken and even smaller ultra-fine mode particles originating in the FT were observed repeatedly in the marine boundary layer during two ship cruises [*Covert et al.,* 1996]. SH (20-70°S) sampling showed that the aerosol size distributions were dominated by the Aitken and ultra-fine mode aerosol, with variability in the SO aerosol concentrations associated with the passage of frontal systems (40-70°S). Aitken and ultra-fine mode particles rapidly subsided from the FT after the passage of a front in these cases and had not grown to larger sizes as they had spent little time in the marine boundary layer (MBL). Because there was no positive correlation between aerosol surface area and the concentrations of ultra-fine particles, it is likely that these particles were formed elsewhere before they were carried into the boundary layer [*Covert et al.,* 1996]. More recent ship observations showed similar behavior: high concentrations of aerosols associated with air descending from the free troposphere over Antarctica [*Humphries et al.,* 2016]. Two SO aircraft transects (August 2016 and February 2017) also found high concentrations of new particles (diameters between 3-7 nm) occurring between altitudes of ~ 3 and 9 km but few new particles in the MBL [*Williamson et al.,* 2019].

How are these new particles produced aloft? One possibility is the occurrence of cloud outflow particle production. These mechanisms have been observed in many regions of the world and across a variety of cloud types (as reviewed in *Kerminen et al.* [2018]). Particle generation results when air masses rich in precursor gases are cleansed of their accumulation and coarse mode aerosol by cloud droplet scavenging and precipitation processes, reducing aerosol surface area enough to enable new particle formation once the air mass exits the cloud. Only the less water-soluble gases (e.g. DMS [*Seinfeld and Pandis*, 2006]) will survive cloud processing, so it is likely that oxidation of gases to particle precursors happens upon exiting the cloud. Large eddy scale (LES) simulations of new particle formation in cumulus cloud outflow in the South East Pacific demonstrate how gases are processed in these events before gas to particle conversion takes place [*Kazil et al.*, 2011]. Based on this study, in marine environments it is likely that DMS fluxed from the surface is lifted through clouds before oxidizing into precursor gases (e.g. SO_2 and then H_2SO_4 and MSA) upon exiting the cloud and being exposed to oxidizing compounds such as OH. Gas to particle conversion will happen shortly thereafter, assisted by the exposure to increased actinic flux, colder temperatures, and high relative humidity [*Seinfeld and Pandis*, 2006] in cloud outflow regions.

Ultra-fine and Aitken mode aerosols formed in cloud outflows can subsequently descend, grow, and be incorporated into the MBL to contribute to the CCN budget. *Clarke et al.* [1998] made an important comparison between particle generation in outflows from SO shallow cumulus and from deeper convective clouds in the tropics, arguing that in the tropics, particles descend from higher and more slowly, allowing time for coagulation and growth. This factor, along with residence time in the MBL [*Covert et al.,* 1996], affects how many aerosols grow to CCN sizes.

Deep convective clouds have been found to be an important source of new particles in numerous locations across the world [*Kerminen et al.*, 2018]. An examination of deep convective

clouds associated with a mesoscale convective system spanning the United States estimated that new particles formed subsequent to cloud uplift in such systems contribute substantially to upper tropospheric aerosol concentrations in the mid-latitudes [*Twohy et al.*, 2002]. In the SO, particle formation, likely from nucleation of co-occurring sulfuric acid, has been observed at the edges of frontal cloud systems [*Weber et al.*, 2001]. We posit that deep stratiform cloud types in the Southern Ocean might also be producing new particles, which suggests that deeper clouds may be contributing significantly to the persistently high concentrations of small particles observed throughout the depth of the SO free troposphere.

In this paper, we show evidence for widespread recent particle formation occurring in free tropospheric air sampled at a range of altitudes up to 6 km during the Southern Ocean Clouds Radiation and Aerosol Transport Experimental Study (SOCRATES) campaign from January – February 2018 off the coast of Tasmania. SOCRATES sampled clouds and aerosols in the cold sectors of Southern Ocean cyclones between 45-62°S. This is a regime in which large concentrations of small aerosols have been observed in the past [*Covert et al.*, 1996] with sulfuric acid signatures consistent with new particles observed aloft [*Weber et al.*, 2001]. In SO cyclone cold sectors, global weather and climate models tend to simulate low clouds that do not reflect enough radiation to space [*Bodas-Salcedo et al.*, 2016; *Bodas-Salcedo et al.*, 2012; *Bodas-Salcedo et al.*, 2014; *Williams et al.*, 2013]. Excessive glaciation of mixed-phase clouds is one explanation, but another contributor may be biases in CCN concentrations, droplet number concentrations, and the aerosol cloud interactions driving these populations [*Bodas - Salcedo et al.*, 2019; *I L McCoy et al.*, 2020 in press; *Revell et al.*, 2019]. SOCRATES was designed to expand our knowledge of the aerosol sources and sinks in these cold sectors and help us better understand Southern Ocean cloud-aerosol interactions.

We pose two questions in our analysis: what is the mechanism for producing the copious quantities of Aitken mode sized particles over the SO (3.1)? And how do these small aerosols influence the clouds in this pristine environment (3.2)? We begin by describing our analysis methodology, datasets, and models (2). We conclude by discussing the implications of free tropospheric aerosol particles influencing SO clouds and how that informs state of the art climate models.

2 Materials and Methods

2.1 Aircraft Sampling

In the SOCRATES campaign [*McFarquhar et al.*, 2020 submitted], the National Science Foundation Gulfstream-V (GV) aircraft flew out of Hobart, Tasmania, over the SO. Fifteen flights (Figure 1a) were designed to sample low clouds in the cold sectors of cyclones. Each research flight (RF) had a similar sampling strategy (Figure 1b). Initially, the GV flew a high (~6 km altitude) survey leg into a region forecast to be dominated by low clouds until a southernmost latitude was reached, typically 60-62°S. The cloud radar, lidar, and dropsondes were used to probe the underlying cloudy boundary layer. After descending to an altitude above cloud (typically ~3 km), the GV returned to Hobart while sampling the boundary layer through repetitions of a flight module. Each module consisted of 10-minute level legs above cloud, in cloud, and below cloud at 150 m above the sea surface, followed by sawtooth profiling through the boundary layer. Module sampling was continued as long as operational constraints allowed, after which the plane climbed back above the boundary layer to return to Hobart. There were two exceptions to this method during the campaign: RF11 and 15 had flight paths customized for

targeting cumulus cloud tops to sample mixed-phase microphysics. The limited observations obtained north of 45° S are affected by proximity to Tasmania. Thus, our analysis focuses on the SO sampled between 45 and 62°S.

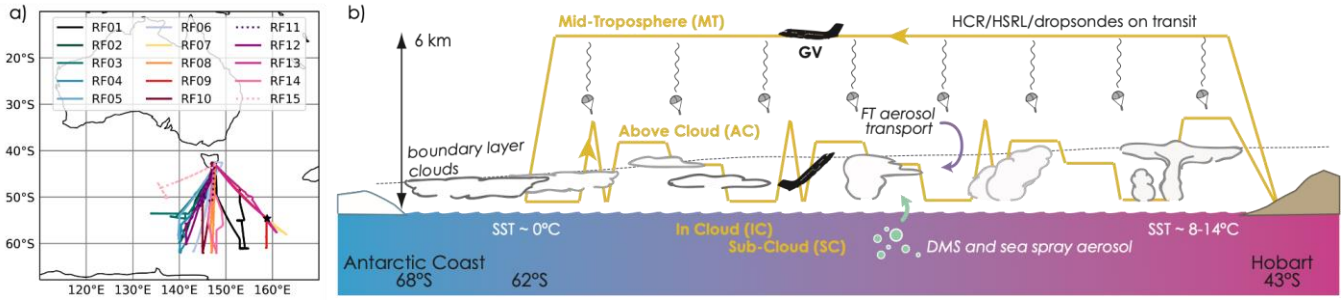

Figure 1 a) Flight locations from SOCRATES (dashed lines for cumulus targeting flights, solid for standard modules) and b) standard flight module plan with identified leg components. Macquarie Island ,a coordinated site for ground observations as detailed in McFarquhar et al. [2020 submitted] is marked with a star in (a).

The GV was equipped with a wide array of instrumentation [*McFarquhar et al.*, 2020 submitted]. The low-rate, 1 Hz flight, state, and microphysical data from the GV was used in this analysis [*Laboratory*, 2019]. The cloud droplet number concentration (N_d) is from the cloud droplet probe (CDP). Aerosol number concentrations are taken from two instruments for our analysis, a condensation nuclei counter (CN, all aerosols with diameters larger than ~0.011 μm) and a ultra-high sensitivity aerosol spectrometer (UHSAS or UHSAS100 when adjusted to the accumulation size range of 0.1 – 10 μm from the nominal size range of 0.085 – 1 μm). The models used were a TSI-3760A condensation nucleus counter on a HIAPER modular inlet and DMT UHSAS-A, S/N 001. The UHSAS provides both size-resolved and integrated concentrations within this range. Size resolved number concentrations for coarse mode aerosol are from the CDP (2 – 50 μm). The surface area reported in this paper is computed from the coarse and accumulation mode size distributions, accounting for particles with diameters between 0.085 and 50 μm. Because UHSAS reports a dried aerosol diameter, surface area is adjusted for swelling associated with the environmental relative humidity. We use the growth factor reported for extinction coefficients, f_{grow}, in eq. 3 of *Chand et al.* [2012]. We then scale this factor by 2/3 to account for surface area growth instead (*personal communication Mike Reeves, NCAR*):

$$SA_{UHSAS} = (\pi D^2_{UHSAS})\left(1 + f^{2/3}_{grow}\right) \qquad eq.\ 1$$

As in *Chand et al.* [2012], the values assumed in calculating f_{grow} are for sulfate aerosols which have a growth factor between sea salt and pollution aerosols. This is not an unreasonable assumption as sulfate or sulfur-based aerosols were the most frequently occurring throughout the campaign (3.1.3).

All aerosol measurements are subject to screening by a cloud and rain mask based on the CDP and the two-dimensional optical array probe (2D-C). Aerosol observations were discarded when our empirically chosen thresholds were exceeded: liquid water content from the CDP ≥ 0.01 g m^{-3} or precipitation droplets from the 2DC ≥ 1 L^{-1} [*Bretherton et al.*, 2019]. Samples were removed for 10 seconds following detection of cloud or drizzle to avoid measurement contamination. Measured temperature and pressure are used to adjust aerosol concentrations to mg^{-1} from cm^{-3} to account for volume changes at different levels in the atmosphere. Cumulative

size distributions are calculated from the drizzle and cloud screened aerosol number concentration for CN, size resolved UHSAS, and size resolved CDP.

We use aerosol measurements behind a counterflow virtual impactor (CVI) [*Noone et al.*, 1988; *Twohy et al.*, 1997] to understand aerosol composition using two approaches: i) scanning transmission electron microscopy (STEM) and X-ray analysis of particles impacted on formvar carbon grids for particles above, in, and below cloud as in *Twohy et al.* [2013], and ii) reconstructed particle volatility estimates from comparing CVI heated CN (using a TSI-3010 condensation nucleus counter, CN_{CVI}) and UHSAS100 (using a UHSAS-G, S/N 15 as in *Kupc et al.* [2018], $UHSAS100_{CVI}$) measurements to un-heated CN, UHSAS100 measurements for free tropospheric particles. Specific examples from the SOCRATES STEM analysis will be highlighted here; for complete details see *Twohy et al.* [2020 submitted]. Normally, the CVI preferentially separates cloud droplets using a counterflow out the tip. For out of cloud, ambient aerosol measurements the counterflow is turned off. The CVI has two primary heaters that can affect particle volatility, one on the probe and one on the long sample line. The CVI probe was heated to ~50-60°C for the majority of the flights to evaporate water and prevent icing when sampling inside supercooled clouds. Because of the instrument and inlet configuration required on the GV, a 4.5m line heated to ~40°C was run between the inlet of the CVI and the instrument rack. The total residence time in the CVI probe and sample line is 2.3 seconds. During their passage through the heated probe and sample line, smaller, more volatile ambient aerosol particles are evaporated. The result of this setup is that for the majority of flights during the campaign the instruments behind the CVI sampled only particles not volatile at ~50°C. During the second half of the campaign, the temperature of the CVI instrument was varied between ~25-60°C to allow for a more detailed investigation of the particle volatility observed. Particles have volatilized in this arrangement when their diameter is reduced to below the CN_{CVI} detection limit (11 nm). Since the CVI has two primary heated regions, the instrument (probe and tip) and sample line, and they behave differently when the heaters are turned off, the maximum of these three temperatures is used for estimating the volatility temperature (i.e. CVI tip, probe, and sample line). Because this analysis approach was not foreseen, the volatilization estimates produced are inexact but still useful.

We use observations from the 2015 Cloud System Evolution in the Trades (CSET) campaign [*Albrecht et al.*, 2019] in the North East Pacific (NEP) to provide a sub-tropical comparison for SOCRATES. This comparison follows in the footsteps of *Clarke et al.* [1998] in establishing the uniqueness of Southern Ocean observations. CSET sampled the stratocumulus to trade cumulus transition between California and Hawaii using a similar modular strategy as in SOCRATES for sampling the cloudy boundary layer. In CSET, the GV used similar wing-mounted instrumentation to SOCRATES, including the CN, UHSAS, CDP, and 2DC [*Laboratory*, 2017]. This allows a parallel data screening and analysis methodology to be applied to both campaigns.

The CSET and SOCRATES flight paths approximately fall along common distance axes. During CSET, this axis was a diagonal line between the coast of California and Hawaii [*Bretherton et al.*, 2019]. During SOCRATES, the axis was roughly a north-south line between Hobart, Tasmania and the coast of Antarctica (Figure 1a). Average structures describing the mean profiles along these axes are developed for analysis. Observations for each flight are sorted into 500 m altitude layers, projected along the appropriate axis, and the median value for the variable in question is computed for each 2.5° bin. Only bins with at least ten 1 Hz flight observations are considered and aerosol samples are subject to the same precipitation and cloud

screening as described above. Along with deriving individual flight composites, these individual composites are averaged together to develop a mean campaign composite as in *Bretherton et al.* [2019]. These gridded structures are particularly useful in comparing variables not sampled simultaneously, such as cloud droplet number and aerosol concentrations.

2.2 Air-mass Back Trajectories

Interpreting SOCRATES aerosol observations requires knowledge of their air mass histories. We used the Hybrid Single Particle Lagrangian Integrated Trajectory (HYSPLIT) model [*Stein et al.*, 2015] to provide this context. HYSPLIT back trajectories were based on Global Data Assimilation System (GDAS) meteorology on a 0.5° by 0.5° grid. Seventy-two hour back-trajectories were calculated for each 10-minute flight segment, based on the aircraft altitude, latitude, and longitude at the mean segment time. The maximum CN concentration for the flight segment (CN_{Max10}) was used to identify likely instances of recent particle formation (RPF) since very high CN is indicative of RPF events in this pristine environment. We split the campaign trajectories by CN_{Max10} quartiles: the upper quartile ($CN_{Max10} \geq 2500$ mg^{-1}) is considered to be comprised of RPF cases and the lower three quartiles ($CN_{Max10} < 2500$ mg^{-1}) are considered unclear or non-RPF cases. This RPF identification method allows us to statistically analyze air mass histories. *Clement et al.* [2002] assessed timescales for sulfuric acid particle formation and growth and found that recently formed particles in the upper troposphere will be observable (~12.5-30 nm) within ~5 hours. Because both the instrumentation and exact conditions of this study (i.e. in the outflow of a mid-latitude storm system) are different from the FT events during SOCRATES, a more appropriate time estimate for when recently formed particles is likely ~10 hours, the upper end of the estimation from *Clement et al.* [2002].

2.3 Nudged Global Climate Model Simulations

A goal of both the SOCRATES and CSET campaigns was to evaluate the fidelity of current global climate models (GCMs). One central strategy was to compare campaign observations with reanalysis-nudged hindcasts from GCMs, as applied by *Bretherton et al.* [2019] for CSET. This approach is applied for SOCRATES to evaluate version 6 of the Community Atmosphere Model (CAM6), which uses the MAM4 aerosol scheme detailed in *Liu et al.* [2016]. CAM6 SOCRATES simulations and microphysics are described in detail by [*Gettelman et al.*, 2020 submitted]. CAM6 is nudged by wind, temperature, and surface pressure fields from MERRA2 reanalysis [*Gelaro et al.*, 2017] with a 1-day relaxation timescale. This ensures the large-scale structure of simulated storms are close to the reanalysis, enabling simulation of similar profiles of clouds, humidity, and aerosols in the model when compared to aircraft observations at a given location and time. Clouds, humidity, and aerosols are not nudged in CAM6, allowing a critical appraisal of their accuracy using the GV measurements. CCN at ~0.6% super-saturation is determined to be the nearest analog to UHSAS100 (which was measured at a fixed super saturation close to ~0.6% during SOCRATES) for these simulations. CN is the sum of aerosol number concentration for coarse, accumulation, and Aitken mode. Both aerosol variables include in and out of cloud values from the model. Cloud droplet number concentration is reported as in cloud. Here we focus on comparing the measured aerosols and cloud droplet number concentrations with CAM6.

3 Results

3.1 Synoptically Generated Recent Particle Formation

3.1.1 Observations of Recent Particle Formation in the Southern Ocean and Sub-Tropics

Frequent high concentrations of small aerosol particles were observed in SOCRATES throughout the depth of the SO free troposphere. Bursts of high CN concentrations with simultaneously low UHSAS100 concentrations were observed in the mid troposphere (~6 km) and above cloud (~3 km) on many of the flights. The high total aerosol concentrations are dominated by predominantly small particles with diameters of 0.01 to 0.1 μm, observed as the difference between CN and UHSAS100, which provides evidence for relatively recent particle formation.

Two example flight segments have been selected to highlight typical signatures that we interpret as evidence for RPF: one segment from a mid-tropospheric survey leg (Figure 2b, 6 km altitude, 1200 km long) and the other from an above cloud leg (Figure 2a, 3 km altitude, 300 km long). The first signature of RPF events is high CN (often exceeding 2500 mg^{-1}) that is rapidly varying, often with up to tenfold changes in concentration over a few km. The CN variability may be a marker of bursts of particle formation or boundaries between different air masses at different stages of nucleation [*Clement et al.*, 2002]. This is often accompanied by an anticorrelation between UHSAS100 accumulation mode and CN concentrations, a sign of particle formation events [*Covert et al.,* 1996]. Finally, particle surface area estimated from the coarse and accumulation mode is below 10 μm^2 mg^{-1} in these segments, a threshold associated with new particle formation [*Covert et al.*, 1996]. This low surface area is common in the SO free troposphere but very uncommon in the underlying boundary layer. Note that RPF events identified by the CN_{Max10} criteria (2.2) are marked for reference.

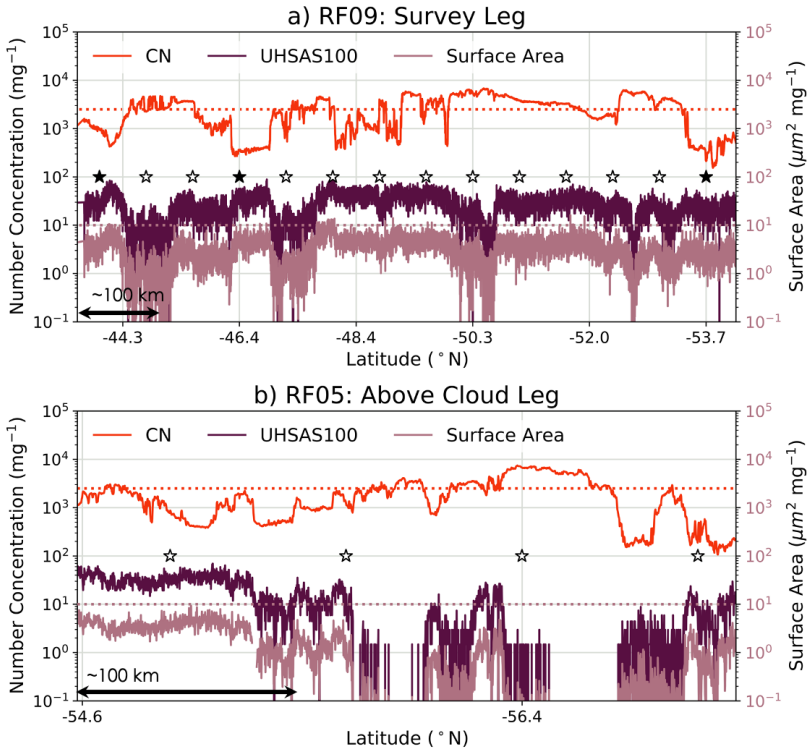

Figure 2 Example cases for suspected RPF events observed in (a) survey-leg sampling in the mid-troposphere during RF09, and (b) above cloud leg sampling during RF05. Observations are shown against time as flight proceeded south (note difference in length scale between a and b). Number concentrations (left) for total (CN, orange) and accumulation mode (UHSAS100, purple) particles. Surface area for coarse and accumulation mode aerosol (right, pink). Dotted lines for 2500 mg^{-1} (orange) and 10 μm^2 mg^{-1} (pink) are included for reference. HYSPLIT trajectory initial locations are marked, solid stars for likely non-RPF events (CN_{Max10}>2500 mg^{-1}) and open stars for regions of suspected RPF events (CN_{Max10}>2500 mg^{-1}). Trajectory altitude profiles are shown for the segment of RF09 in (a) in McFarquhar et al. [2020 submitted].

Outflow from cumulus congestus rising above the mean boundary layer is known to be a region of new particle formation in the SO [*Clarke et al.*, 1998]. SOCRATES sampled in or downwind of such regimes only infrequently. However, high particle concentrations, suggesting recent RPF events, were observed at all elevations of the free troposphere, as is shown in the following height-based separation analysis. SOCRATES data is split into sampling from the mid-troposphere (MT: $Z \geq 4.5$ km, a and b), above-cloud (AC: $1.5 \leq Z \leq 4.5$ km, c and d), and sub-cloud (SC: $Z \leq 1.5$ km, e and f) regions (as in Figure 1b). At each level, normalized pdfs of CN and UHSAS100 are computed. Results are shown in Figure 3 along with CSET observations that will be discussed subsequently. In both the MT and AC sampling, a significant percentage of SOCRATES samples have CN well above 1000 mg^{-1} (Figure 3b, d). The UHSAS100 PDF at these levels shows infrequent concentrations in excess of 100 mg^{-1}, indicating these high CN concentrations are mainly Aitken mode particles (Figure 3a, c). Quantifying the 1000 mg^{-1} and above range gives us information about both the recently formed particles (bursts of which are captured by our stricter RPF event definition for statistical analysis, 2500 mg^{-1}) and the slightly lower concentrations of older, coagulated Aitken particles which still significantly contribute to the total aerosol amount. SC concentrations of CN in excess of 1000 mg^{-1} are less frequent but the PDF still retains significant probability near 1000 mg^{-1} (Figure 3f). As in the MT and AC sampling, the majority of particles SC are smaller than the accumulation mode size range (Figure 3e, f). However, we see a consistent shift with height in the UHSAS100 pdfs: at lower altitudes, the higher UHSAS100 concentrations become more common. The high CN concentrations

become less common SC. This suggests that there is some coagulation and growth occurring as the aerosols descend into the boundary layer (subtly shifting UHSAS100 distributions to higher concentrations). However, CN is not significantly depleted until the SC which indicates cloud processing is key.

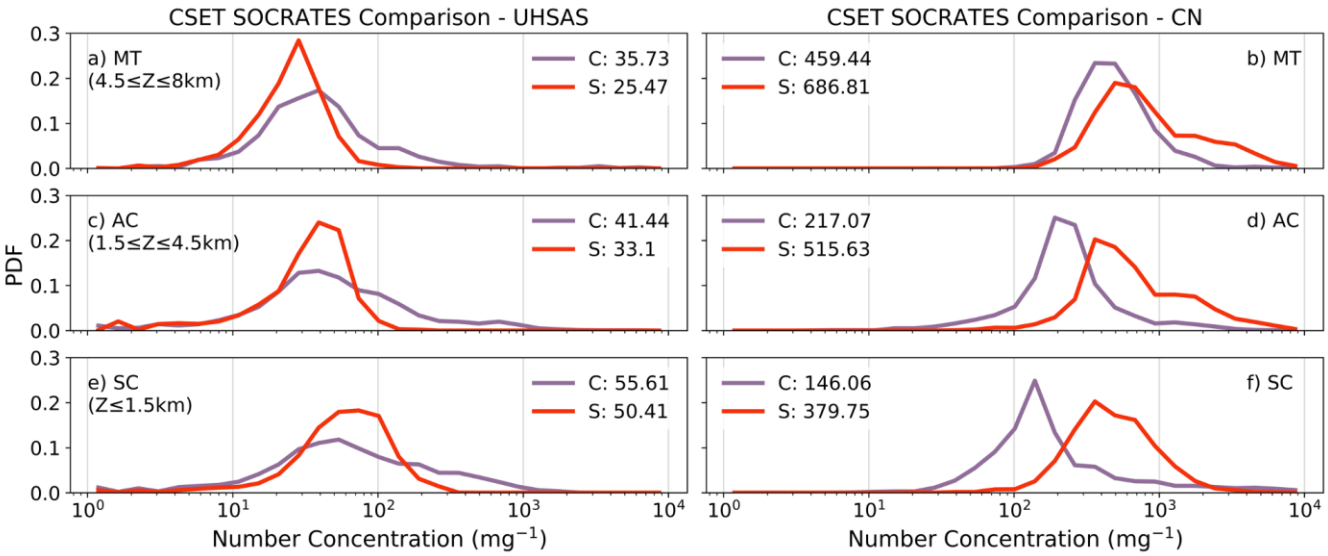

Figure 3 PDFs of number concentrations for UHSAS100 (a, c, e) and CN (b, d, f) for different altitudes: mid-troposphere (a, b), above cloud (c, d), and sub-cloud (e, f). SOCRATES observations (orange) are contrasted with CSET observations (purple).

How different is the SO aerosol structure from the structure in subtropical marine regions and what does that information tell us about new particle production in the SO? We compare height-matched number concentration pdfs for UHSAS100 and CN from CSET at the same levels as in SOCRATES (Figure 3). At all altitude levels there is more accumulation mode aerosol and, because total aerosol concentrations are lower, less Aitken mode aerosol in CSET than in SOCRATES. Accumulation mode aerosols have a wider range of high concentrations that can occur in the subtropics compared to the SO (Figure 3a, c, e), potentially affecting the variability in N_d and cloud albedo in these regions. Lower and less variable CN concentrations typify CSET compared to SOCRATES. SC CN campaign pdfs are the most separated (Figure 3f) while MT CN pdfs are the most similar (Figure 3b).

If local wind-driven sea-spray production was primarily responsible for driving below cloud aerosol number production, we would expect a higher ratio of accumulation to Aitken mode aerosol concentration in SOCRATES where winds were stronger compared to CSET. However, this is opposite to our observations (Figure 3e, f) which suggests that primary aerosol production is not the largest contributor to the heightened aerosol concentrations in the SO. While number may not be linked to wind speed production, increased surface gas emissions associated with higher wind speeds [*Lana et al.*, 2011] may still be assisting in secondary aerosol production and in growing SO aerosols.

In CSET, much more than in SOCRATES, the relative humidity was typically low (10-50%) at 6 km, implying a height of last saturation above 8 km, consistent with outflow from deep convective clouds [*Clarke et al.*, 1998; *Williamson et al.*, 2019] or midlatitude cyclones. Previous studies imply that particles generated in this outflow coagulate as they slowly descend [*Clarke et al.*, 1998; *Williamson et al.*, 2019], which may lead to the higher UHSAS100 concentrations aloft during CSET (Figure 3a). This aging process would also explain the lower

frequency of high CN concentrations for CSET in the MT and AC compared to SOCRATES (Figure 3b, d). The higher SOCRATES concentrations indicate SO aerosol is more recently formed at these levels while CSET is sampling aging aerosols as they descend from nucleation events above 6 km. The vertical aerosol concentration gradients in CSET suggest coagulation and growth processes occur more significantly in the sub-tropics than the SO: UHSAS100 pdfs shift to larger concentrations and CN to smaller concentrations with descent during CSET. Hints of this process are seen in SOCRATES but they are muted compared to CSET (e.g. compare Figure 3c, d to e, f).

3.1.2 Evidence for Particle Generation through Synoptic Uplift Mechanism

We have established that there are frequent and remarkably high concentrations of small, Aitken mode aerosol particles occurring in the lower free troposphere over the Southern Ocean. But how are they forming? Based on previous studies in the SO [*Clarke et al.*, 1998], it is likely that the outflow regions from low, cumulus clouds are contributing to the high Aitken mode concentrations observed above cloud (~3 km) during SOCRATES. This mechanism does not explain the high Aitken mode concentrations observed in the mid-troposphere (~6 km) or the high concentration of particles observed at the surface. In the sub-tropics and mid-latitudes, new particles have been observed in outflow regions of deep convection [*Kerminen et al.*, 2018]. However, high concentrations of small particles were observed on most SOCRATES flights and across a range of weather regimes with little evidence of recent penetrative congestus convection upstream. There was also little evidence of sub-cloud particle formation signatures during SOCRATES.

Based on evidence gathered during SOCRATES and a synthesis of evidence presented in the literature (1), we propose that a novel variant of the cloud-outflow mechanism for particle formation is at work in the SO: new particles are formed and dispersed after boundary-layer air is lifted and processed through precipitating stratiform clouds forming in regions of synoptic scale ascent. Two vital steps for gas to particle formation are occurring in this synoptic-uplift mechanism: i) the total surface area of the particles in the air is being reduced through uplift and rain out associated with clouds and ii) DMS lofted from the surface is given the opportunity to undergo photochemical reactions and nucleate into new particles rather than depositing onto existing aerosol particles. Increased actinic flux and cold temperatures experienced aloft in cloud outflows also assist the photochemical processing of DMS oxidation products and encourages particle formation. This mechanism is consistent with earlier observations of new particles and sulfuric acid vapors in the outflow of a frontal system off of Tasmania at ~6 km during ACE-1 [*Weber et al.*, 2001].

To test the synoptic uplift mechanism, we examine the altitude history of the mid-tropospheric air masses sampled in SOCRATES using RPF and non-RPF identified HYSPLIT 72-hour back trajectories (Figure 4a, b) (2.2). RPF air masses typically have a much steeper composite ascent profile over the past 72-hours compared to the non-RPF composite profile (Figure 4a). During the ascent period (10 to 70 hours back), the rate of ascent of the RPF cases (1.1 cm s^{-1}) is comparable with the characteristic vertical velocity for mid-latitude synoptic systems (~1 cm s^{-1}) [*Hakim*, 2013] while the non-RPF cases are slower (0.6 cm s^{-1}). The depth and the steepness of the ascent is a marker of uplift through clouds, which will result in cloud processing and precipitation removal of accumulation and coarse mode aerosol in the air masses. RPF cases also come from below 1 km more frequently in the proceeding 72 hours compared to

non-RPF cases (Figure 4b). This indicates that RPF trajectories are able to source the necessary precursor gases (e.g. DMS) from the boundary-layer for gas to particle conversion to take place.

Above cloud RPF events are similarly examined (Figure 4c, d). There is a clear distinction between the RPF and non-RPF cases in the 48 hours prior to sampling: RPF cases have rapid synoptic (1 cm s^{-1} in the last 20 hours) and presumably saturated ascent profiles (Figure 4c) and come from below 1km (Figure 4d). On average, the non-RPF trajectories undergo less total ascent, do not come from as near the surface, and ascend earlier. The latter results in longer residence time in the boundary layer where Aitken aerosols grow and coagulate to accumulation mode sizes, depleting their CN.

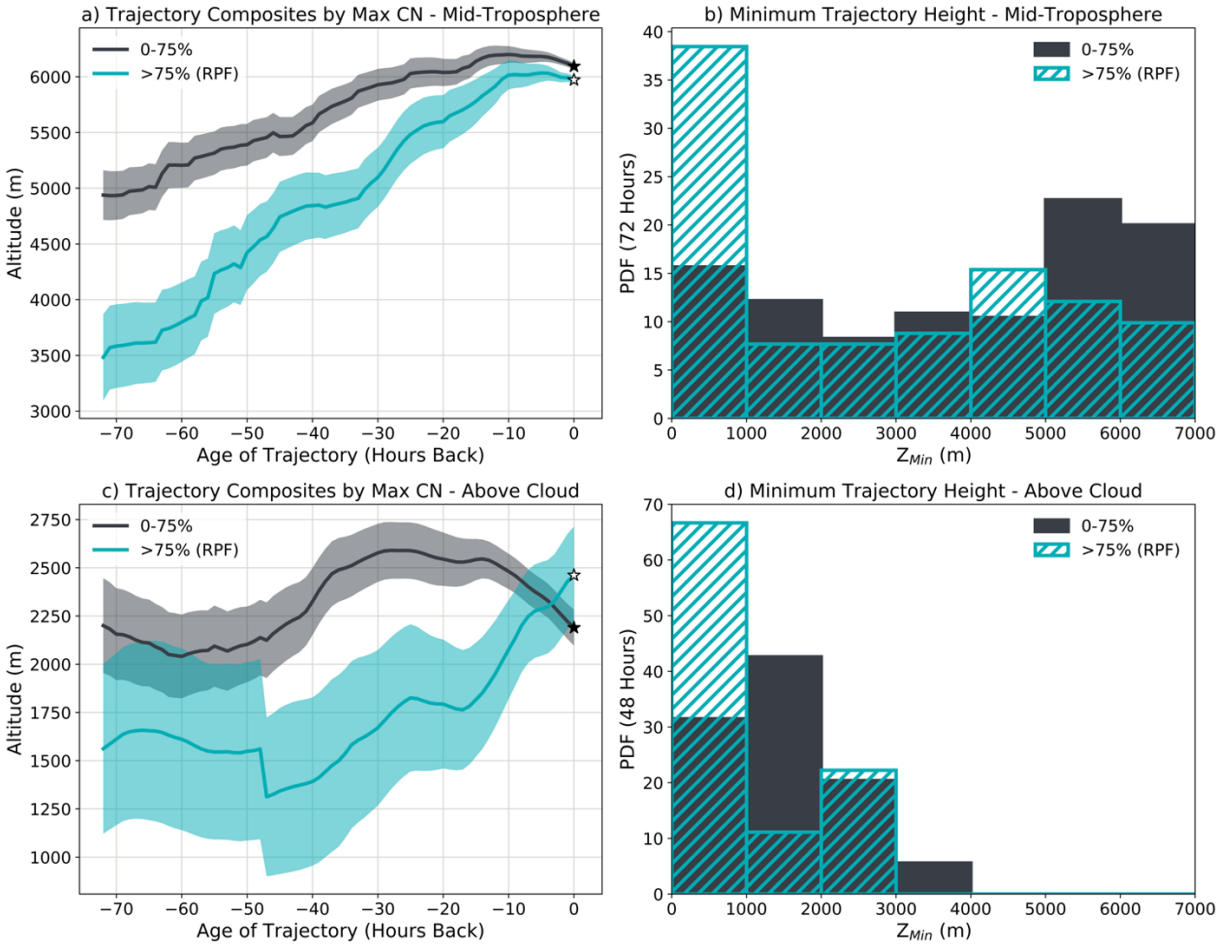

Figure 4 Mean (line) and corresponding standard error (shading) of ascent profiles for HYSPLIT trajectories initiated in the mid-troposphere (a) and above cloud (c). Corresponding distribution of minimum height over proceeding time where altitude profiles are statistically distinct: 72-hours for mid-troposphere (b) and 48-hours for above cloud (d). Trajectories are composited by CN_{Max10} into RPF events (blue, CN_{Max10}>75%) and non-RPF events (gray, 0-75% CN_{Max10}). Number of RPF vs non-RPF cases per SOCRATES research flight for mid-troposphere and above-cloud are shown in Figure S1.

What are the large-scale synoptic patterns leading to rapid uplift over the SO? We employ ECMWF ERA-5 reanalysis to understand the large-scale motions associated with the HYSPLIT trajectory ascents. RF07 is used as an example case for identifying synoptic patterns because many RPF back-trajectories were identified from the 6 km survey leg during RF07, each with a rapid ascent profile (Figure 5a). Rapid ascent from the boundary layer occurred in two periods, one at ~60 hours (Figure 5b) and the other at ~36 hours (Figure 5c) prior to GV

sampling. We use vertical velocity and geopotential height fields at 700 hPa (chosen as a representative mid-level altitude) to identify the cause of uplift: a warm conveyor belt (WCB). A representative geopotential height contour traces the backbone of the eastward propagating Rossby wave occurring in the Southern Ocean during this case. The complete 72-hour evolution of this case is included as an animation of maps in 3 hourly snapshots (MS01). At 60 hours back (Figure 5b), a tongue of warm, moist air from the sub-tropics is advected up and poleward ahead of the cold front, lifting the boundary layer air up towards the mid-troposphere (42°S, 54°E). At 36 hours back (Figure 5c), trajectories near the phytoplankton-rich ocean off the edge of Antarctica (60°S, 100°E) undergo uplift associated with the remains of the WCB that has traveled along the Rossby wave.

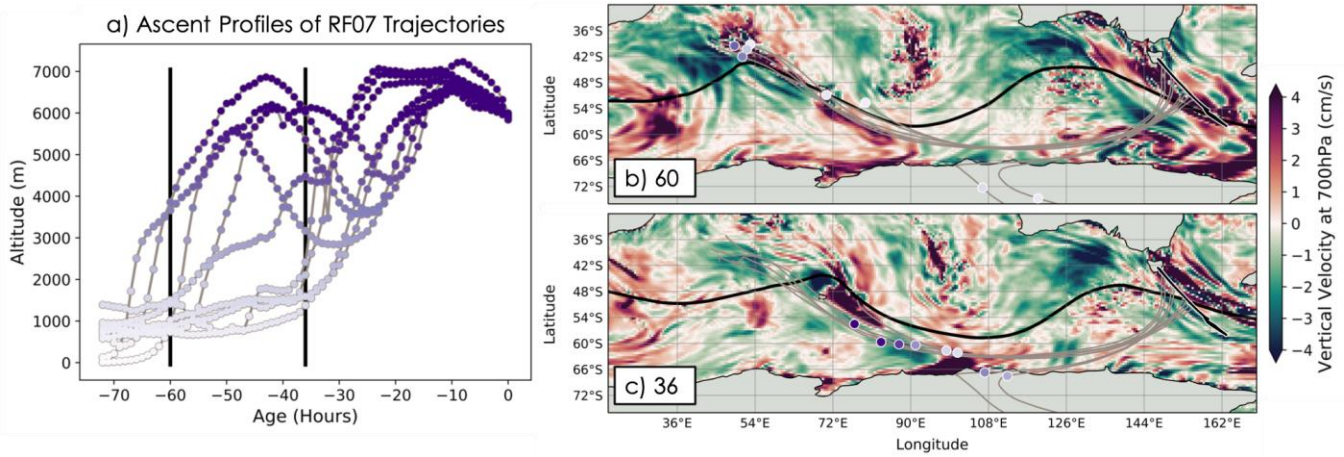

Figure 5 Illustration of synoptic scale patterns influencing mid-tropospheric RPF identified air masses sampled by RF07 (black line from Tasmania, b and c). Two times of uplift are highlighted in the ascent profiles (black lines, a) and shown in reanalysis snap shots: 60 (b) and 36 (c) hours back from time of GV sampling. ERA5 reanalysis maps include 700 hPa vertical velocity (colors) with a 700 hPa geopotential height contour of 2.9 km for reference (black contour). In general, the contour separates warmer, moister sub-tropical air from cooler, drier polar air. RPF trajectories (gray lines) with air mass locations (circles) colored by their altitude (white to purple, as in the ascent profiles in a). Ascent of the first set of trajectories at 60-hr (b) occurs off the tip of Africa while ascent of the 36-hr trajectories (c) occurs off the coast of Antarctica, both driven by the advance of a warm-conveyor belt towards the south east (i.e. along the height contour). Note sub-polar vortices affecting the vertical velocity in c) at 60°S, 72°E and 54°S, 140° E. Animation of RF07 synoptic event included in supplemental material (MS01).

The WCB during RF07 generated regions of potential vorticity anomalies resulting in upward motion. While they did not affect the trajectories sampled during RF07, sub-polar vortices (e.g. 60°S, 70°E and 54°S, 140°E, Figure 5c) lead to uplift of boundary layer air to the mid-troposphere in other research flight cases. We concluded from analysis of all SOCRATES flights that the uplift along RPF trajectories is typically associated with either warm conveyor belts or sub-polar vortices.

In the southern hemisphere, WCBs are not always associated with cyclones [*Catto et al.*, 2015]. Climatology of WCB features show a high frequency of events occurring off the tip of South America and South Africa [*Catto et al.*, 2015]. WCBs are also not as constrained in longitude in the Southern Hemisphere as in the Northern Hemisphere and occur frequently across a wide range of longitudes in the SO [*Eckhardt et al.*, 2004]. The behavior of mid-tropospheric RPF trajectories is consistent with both these characteristics of WCB behavior in the SO: i) the typical RPF trajectory path arcs down from South Africa towards Antarctica, funneling along the large-scale waves in the region, and ii) the geographic location of minimum RPF trajectory altitude is widespread across the SO (Figure S2).

Synoptic-scale uplift is frequent over the Southern Ocean and can set the stage for new particle formation aloft. The pattern of minimum RPF trajectory altitude is similar to the pattern of climatological DMS fluxes for January and February, with particular hotspots occurring off the tip of Africa, edge of Antarctica, and, in general, to the west of Australia and up-wind of the SOCRATES sampling locations [*Lana et al.*, 2011]. The collocation of synoptic uplift regions and DMS-rich boundary-layer air provides the precursor gases and aerosol cleansing necessary for frequent occurrence of gas to particle formation in the free troposphere and ensures that RPF is widespread across the SO. We propose that this mechanism frequently produces new particles throughout the lower free troposphere. Figure 6 presents a conceptual diagram for aerosol cycling over the SO associated with this uplift mechanism and the cumulus outflow mechanism, augmented from a similar diagram in *Clarke et al.* [1998].

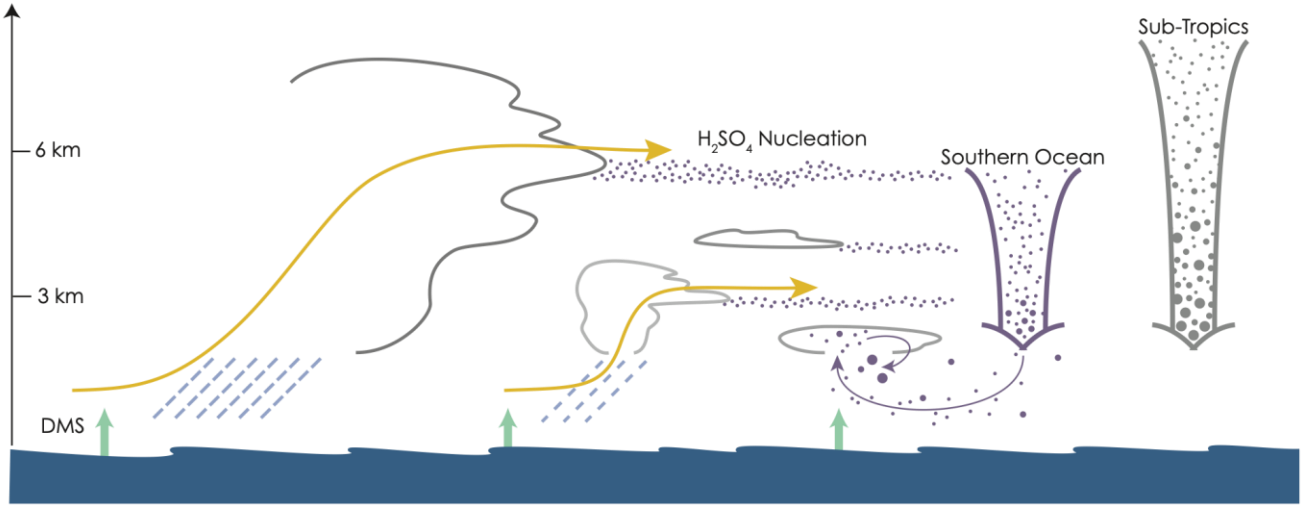

Figure 6 Diagram of synoptic uplift mechanism for generating new particles. As in Clarke et al. [1998], differences in the distribution of aerosols between the Southern Ocean (purple) and sub-tropics (gray) are highlighted.

3.1.3 Southern Ocean Summertime Aerosol Composition Estimations

If new particle formation generated through synoptic uplift (Figure 6) is significantly impacting the formation of free tropospheric aerosols, we expect to find signatures of DMS oxidation products in the particles sampled. In this section, we use ambient aerosol measurements from the CVI (2.1) to illuminate the likely composition of summertime SO aerosols sampled by SOCRATES. We draw two conclusions from this analysis: i) Aitken and small accumulation mode ($\leq$ 200 nm) particles occurring in high number concentration samples in the free troposphere are composed primarily of H_2SO_4 with possible contributions from more volatile DMS oxidation products like MSA, and ii) accumulation-mode particles (~100-500 nm diameter) sampled above, below, and in-cloud are primarily sulfur-based with limited sea spray influence.

Our first conclusion is based in part on a particle volatility estimate drawn from the temperature evolution of the ratio between the condensation nuclei number concentration measured behind a heated CVI (CN_{CVI}) and the unheated measurement from the CN (Figure 7). During the campaign there was limited sampling where both high aerosol concentrations occurred and CVI temperatures were cycled, so our analysis expands beyond RPF cases to all instances where CN $\geq$ 800 mg^{-1}. However, we limit our examination to the free troposphere (Z $\geq$ 1.5 km) because i) the majority of the CVI temperature cycling experiments occurred in this

altitude range and ii) our interest is primarily in the Aitken-mode dominated environments. Median cumulative distributions (2.1) are calculated for each above cloud and mid-tropospheric level leg during the campaign (Figure S3). These demonstrate that free-tropospheric altitudes are dominated by Aitken-mode aerosols (except for a few near-cloud contaminated samples marked by high relative humidity, Figure S3b).

The free-tropospheric, Aitken dominated samples contain predominantly volatile particles. This is exhibited by the decrease in CN ratio with increasing CVI temperature (Figure 7) when the ambient particles (temperatures between -20 and -15°C in the mid-troposphere, -5 and 0°C above cloud) are exposed to CVI temperatures between ~25-60°C, taken as the maximum of several temperature measurements in different parts of the instrument configuration (2.1). The most dramatic number decrease in particles measured by CN_{CVI} occurs when maximum temperatures are above ~25-30°C. The volatilization of Aitken mode particles under this imposed CVI temperature range is consistent with previous volatility analysis for small particles primarily composed of sulfuric acid. *Orsini et al.* [1999] measured the volatility of H_2SO_4 as a function of particle size and found that small particles volatilize at much lower temperatures than larger particles, with a more than 30% decrease in diameter for 15 nm particles at 25°C. *Clarke* [1991] observed that sulfuric acid particles with mass mean diameters of 300 nm began losing mass at about 30°C (disappearing completely by 125°C). Conversely, compounds like neutralized sulfate (e.g. ammonium sulfate) and sea spray aerosol (e.g., NaCl) volatilize at much higher temperatures (> ~200, ~300°C respectively) than H_2SO_4 [*Schmid et al.*, 2002] and thus are unlikely to contribute to the composition of the particles sampled here. This is consistent with other SO observations showing new particle formation largely produces sulfuric acid particles [*Clarke et al.*, 1998; *Weber et al.*, 2001; *Yu and Luo*, 2010] and suggests H_2SO_4 dominates particle composition in the SO free troposphere.

For the limited temperature range maintained over the CVI sample lines during SOCRATES (~25-60°C), we do not expect all sizes of particles to evaporate completely (i.e. shrink below the 11 nm detection threshold of the CN counter) if they are composed purely of sulfuric acid. *Orsini et al.* [1999] found that sulfuric acid particles initially ≥ 35 nm in diameter required exposures to temperatures over 90°C for ~0.2 seconds before their diameters were reduced below 11 nm. For the longer residence time during SOCRATES (~2 seconds), it is likely the temperature required for sub-detection limit volatilization will be reduced but not to below 35°C. Based on this and the strong volatility of Aitken-dominated samples at ~25-30°C (Figure 7), we conclude that if the Aitken mode particles are composed predominantly of sulfuric acid then the majority of particles must be ≤ 20 nm in diameter. This is similar to the size of particles *Orsini et al.* [1999] found evaporated below 30°C and is consistent with findings by *Schmid et al.* [2002] for very small sulfuric acid particles. Unfortunately, a more nuanced discussion of particle volatility by size is not possible for Aitken mode aerosols during SOCRATES due to instrument limitations.

Volatility signatures were also noted in the size-resolved accumulation mode UHSAS measurements during the campaign which provides some additional insight into particle composition. There are very few accumulation mode particles contributing to the Aitken-dominated free-tropospheric samples analyzed in this section (on the order of 50 mg^{-1} or less, Figure S4b) and most are ≤ 200 nm (Figure S3). However, enough UHSAS100 aerosols were sampled during CVI temperature cycles to conduct a limited examination of accumulation mode volatility using a matching ratio analysis to Figure 7 (Figure S4). The UHSAS100 ratio is found to exhibit a decrease near ~25-30°C, similar to the CN ratio although likely noisier due to the

small number of accumulation mode particles sampled. The similarity of the temperature inflection point for these two volatility ratio curves suggests that small accumulation mode aerosols may share their composition with Aitken aerosols in these high aerosol concentration events and that volatile DMS oxidation products are likely the leading contributor to the composition of the few accumulation mode aerosols occurring in the FT (Figure 3a, c).

Intriguingly, the magnitude of the change in particle size in the small accumulation mode range (shrinking from 100-200 nm to below 100 nm) possibly signals the presence of aerosol species with even higher volatility than sulfuric acid [*Orsini et al.*, 1999]. The most likely candidate for an additional, volatile species contributing to particle composition over the SO is MSA, another DMS oxidation product and one with a higher vapor pressure than H_2SO_4 [*Berresheim*, 2002; *Mauldin et al.*, 1999]. Relatively large MSA particles (160-260 nm) have been found to volatilize at ~50-60°C [*O'Dowd et al.*, 1997]. It is thus possible for small, recently formed MSA particles to evaporate at 30-35°C with the increased SOCRATES CVI residence time. MSA may also be contributing to the separation between the above cloud and mid-tropospheric volatility curves (Figure 7, S4). The mid-tropospheric observations from SOCRATES found higher concentrations of Aitken particles (~CN-UHSAS100, colors in Figure 7, S4a), which may mark less coagulation and growth occurring after particle formation and resulting in smaller, more volatile particles. However, mid-tropospheric particles reside at lower ambient temperatures and slightly lower relative humidity (Figure S3a) as well. If MSA is present, this environment could drive MSA to partition preferentially to the particulate phase [*Berresheim*, 2002] where it could dominate the volatility response. Future campaigns outfitted with instruments capable of measuring gas composition and aerosol concentrations with Aitken mode size resolution will help to further demystify these volatility signatures.

We can gain broader insight into accumulation mode particle composition across the SOCRATES campaign from STEM analysis of micro-impactor filters taken during ambient CVI sampling [*Twohy et al.*, 2020 submitted]. Sulfur-based particles are found to dominate the number concentration in the accumulation mode (~100-500 nm) at all altitudes during the SO summer. The remaining number fraction (20-30%) is composed of salt-based sea spray, sometimes enriched with sulfur or other trace compositions, and have a smaller influence on particles sub- and in-cloud compared to the sulfur-based particles. If small amounts of organic material occur in these samples, they are not detectable on the carbon STEM substrate. The composition of these accumulation-mode particles is what one would expect to observe from the growth of sulfuric acid or other DMS oxidation product sourced Aitken mode aerosols and is consistent with our volatility analysis. Implications of Aitken particle growth into accumulation mode sizes will be discussed further in section 3.2.2.

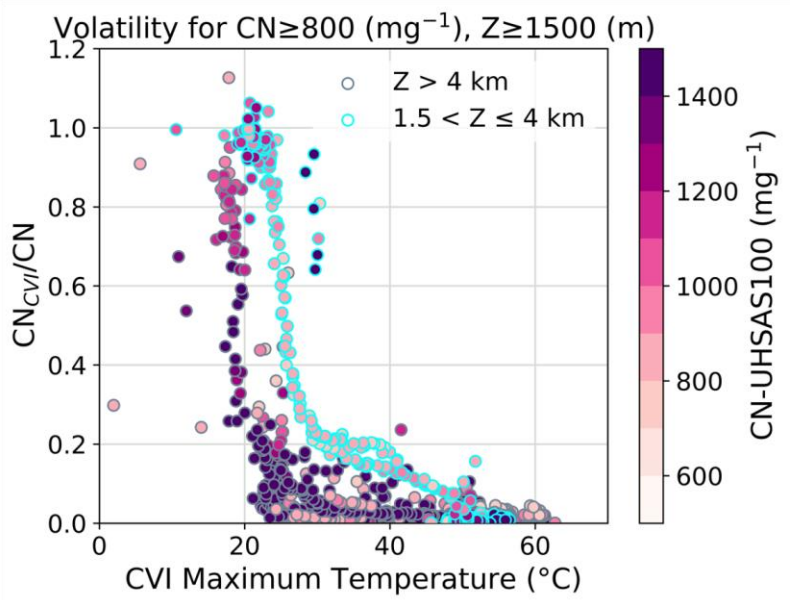

Figure 7 Volatility curves from CVI analysis presented as the ratio between CN and CN_{CVI} versus the maximum temperature of the CVI instrument. Points are shown for CN ≥ 800 mg^{-1} above which the small particle concentration is large enough to mark RPF or slightly grown nucleation mode aerosol. Points are limited to free tropospheric samples (Z ≥ 1.5 km) due both to limited temperature cycling in the boundary layer and to targeting Aitken mode dominated environments. Outline colors denote altitude of sample: mid-troposphere (gray) and above cloud (blue). Points are colored by CN-UHSAS100 to estimate the number of particles in the Aitken mode (generally more in the mid-troposphere).

3.2 Controls on Southern Ocean Aerosol and Cloud Droplet Number Concentrations

3.2.1 Average Southern Ocean Aerosol and N_d Structures

To better understand the factors influencing the generation and depletion of aerosols and cloud droplets in the SO and how synoptically generated Aitken particles influence the SO aerosol budget, it is useful to examine the spatial distribution of aerosol and cloud features. Using the altitude by latitude binning methodology (2.1), a multi-flight, campaign average composite is generated for aerosol and cloud droplet number concentrations (Figure 8).

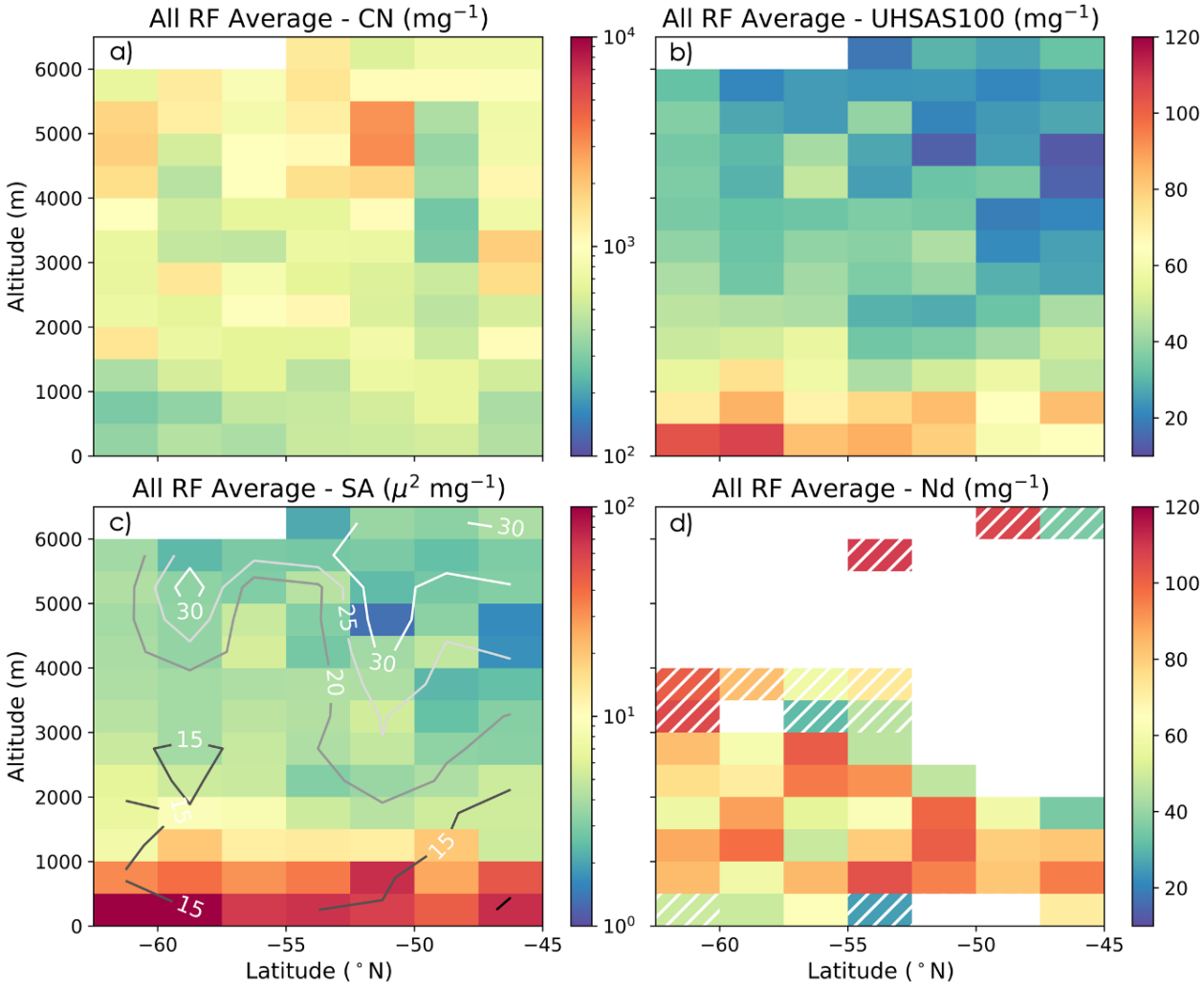

Figure 8 All flight average composites of binned flight medians for 500m x 2.5° boxes. Aerosol variables are screened for cloud and rain contamination. Number concentrations for (a) total aerosol, (b) accumulation mode aerosol, and (d) cloud droplets are shown along with (c) the surface area concentration computed from accumulation and coarse mode size distributions. Contours of all flight average composite wind speed are also included (c). Bins where 2 or less flights sampled are hatched to indicate reliability of sampling. A companion plot to (d) of cloud droplet number concentration in cm^{-3} units is in Figure S5.

The mean SO CN does not vary significantly with latitude and maintains particle concentrations on the order of 1000 mg^{-1} above cloud (≥1.5 km) and 600 mg^{-1} in the boundary layer (<1.5 km) (Figure 8a). This is consistent with the altitude trend in the CN histograms shown in Figure 3 (d, e, f). The prevalence of consistent high concentrations of CN in the free troposphere across all latitudes suggests that the synoptic generation mechanism (3.1) is influential to the Aitken mode concentration throughout the SO.

The accumulation mode aerosol (Figure 8b) and surface area derived from the UHSAS and CDP (Figure 8c) both decrease significantly with altitude and have the largest values in the near-surface bins. Aerosol surface area is higher near the surface due to sea spray production (Figure 8c). There is a slight increase in both surface area and UHSAS in the two most southerly surface bins potentially associated with enhanced wind speed (contours, Figure 8c). However, this does not appear to influence sub-cloud UHSAS (500-1000m).

Surface area is consistently low enough (SA< 10 μm^2 mg^{-1}) above 2 km to support gas to particle conversion [*Covert et al.*, 1996]. The one exception to this was during RF13 under an anticyclonic ridge, where a narrow rift of precipitating shallow cumuli was embedded in an extensive stratocumulus layer. In this instance, low SA and high, variable CN were observed in the rift but not the surrounding stratocumulus-capped MBL.

Droplet number concentration is relatively constant with latitude and varies with altitude (Figure 8c). Cloud observations occur in more altitude bins to the south, possibly a manifestation of the more frequent occurrence of multi-layered clouds in the south of the SO. Most bins average N_d between 60 and 100 mg^{-1} (approximately the same range in cm^{-3}, see Figure S5), similar to climatological N_d from MODIS satellite retrievals in this region and season [*Bodas-Salcedo et al.*, 2019; *Grosvenor et al.*, 2018; *I L McCoy et al.*, 2020 in press]. This summertime concentration is much higher than the average boundary-layer N_d sampled in the austral winter slightly to the north of this region (~32 cm^{-3} between 43-45°S) [*Ahn et al.*, 2018]. This seasonality is consistent with previous work connecting N_d increases with more availability of DMS products and other biological aerosol sources in the SO summertime [*Ayers and Gras*, 1991; *Boers et al.*, 1998; *D T McCoy et al.*, 2015].

What is the source of aerosol influencing N_d? The campaign average N_d is comparable to the sub-cloud UHSAS100 accumulation-mode aerosol concentration (Figure 8b, d). Spatially and temporally matched bins from individual flight composites for N_d and UHSAS100 are well correlated (R=0.62, Figure 9b). Distributions of bin matched and raw flight data match for N_d and UHSAS100, indicating bin averages are representative of cloud and aerosol tendencies (Figure 9a, c). Level-leg median N_d measurements are additionally found to have a stronger relationship with median sub-cloud level leg UHSAS100 (R=0.64) than with above-cloud UHSAS100 (R=0.40). We conclude from these relationships that SO N_d is controlled by sub-cloud accumulation mode aerosol. Thus, a more appropriate question is: what is the source of *sub-cloud* aerosol in the SO that influences N_d?

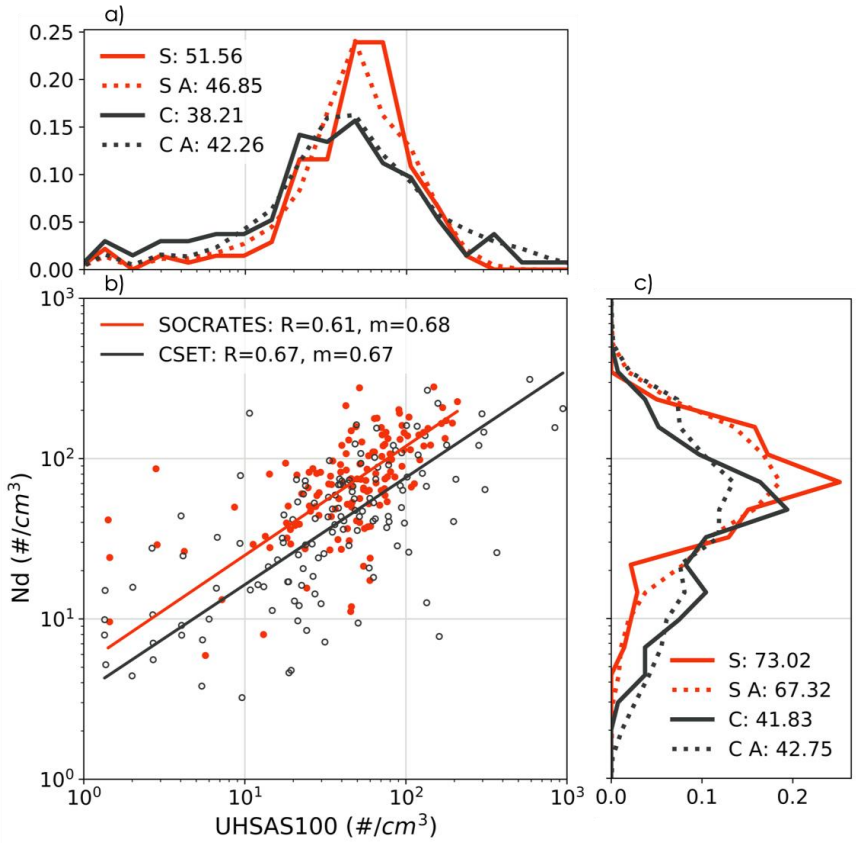

Figure 9 Relationship between accumulation mode and cloud droplet number concentrations in SOCRATES (orange) and CSET (gray). (b) Altitude vs Latitude (SOCRATES) or Longitude' (CSET) 500m x 2.5° bin medians for N_d and UHSAS100 are computed for each flight and compared. PDFs of binned data are shown for (a) UHSAS100 and (c) N_d as solid lines. PDFs of raw flight data for the campaigns are shown as dashed lines (a, c) and agree with the behavior of the binned subset. Corresponding median values are included for reference. Few instances of precipitation-depleted N_d or N_d-UHSAS100 points occur (≤ 10 cm^{-3}) in SOCRATES. CSET has a greater number of precipitation depleted cloud and aerosol features (b, c).

For guidance in answering this question, we can look to another cloudy marine environment heavily influenced by mid-latitude storms and biologically active aerosols: the North East Atlantic (NEA). Recent observations in the NEA found free tropospheric Aitken mode particles descending into the boundary layer and subsequently growing to accumulation modes sizes through surface gas absorption and cloud processing [*Sanchez et al.*, 2018; *Zheng et al.*, 2018]. Similar behavior may be occurring in the SO. The pattern of CN and UHSAS concentrations as well as the heightened SA sub-cloud during SOCRATES suggests i) recent particle formation is the primary contributor to high CN in the free troposphere (UHSAS100 low, CN high) and ii) it is unlikely that there is a strong surface source of CN generating the Aitken particles seen above cloud (CN low sub-cloud, high above-cloud; SA sub-cloud too high for gas to particle conversion). We speculate that CN is depleted through in-cloud processing and growth to UHSAS sizes, reducing to the lower concentrations observed in the boundary layer (600 mg^{-1}). Observations of particle movements during SOCRATES are limited due to the instantaneous nature of the GV sampling, but earlier literature discussed Aitken particles descending from the free troposphere and influencing SO boundary layer aerosol [*Covert et al.*, 1996; *Humphries et al.*, 2016]. Using a global chemical transport model, *Korhonen et al.* [2008] estimated that FT DMS-oxidation product based new particles (i.e. H_2SO_4) entrained into and grown in the MBL contributed between 43-65% of zonal mean CCN in the SH summertime

oceans. This was also determined the dominant microphysical pathway for DMS to influence SH marine CCN. In the next section, we examine SOCRATES observations to further assess the importance of the FT Aitken source on SO summertime sub-cloud CCN concentrations.

3.2.2 Sources of Accumulation Mode Aerosol in the Southern Ocean

We have established that sub-cloud aerosol is significant in controlling cloud droplet number concentration. However, we do not as yet understand the source of this aerosol in the SO. We broadly expect accumulation mode aerosol to be developed from i) primary sea spray emissions from the surface or ii) growth from secondary aerosol emissions such as Aitken mode aerosols (either from the boundary layer or free troposphere). To understand which of these behaviors is dominating, we begin by calculating a cumulative size distribution for sub-cloud aerosol and examining its characteristics (Figure 10). A median cumulative distribution (2.1) is developed for each sub-cloud level leg on each flight and colored by the corresponding median wind speed. Wind speed is a common proxy for estimating sea spray production from waves and sea spray [*Grythe et al.*, 2014] as well as the magnitude of surface gas fluxes. Correlations are calculated between wind speed and the log of the cumulative number concentration at intervals to understand the importance of wind-speed mechanisms at different sizes.

The most notable finding from these wind speed correlations is that wind-speed production mechanisms are an insignificant contribution to overall sub-cloud accumulation mode and Aitken mode concentrations. Coarse mode aerosol number (CDP, 3-30 μm) is positively correlated with wind speed, consistent with the larger SA at the surface and in the southerly bins in Figure 8c. Within the CDP range, the wind speed correlation weakens as aerosol sizes decrease to the accumulation mode range (UHSAS). They then increase again for the larger UHSAS sizes (0.3-1 μm). This suggests particles in these larger size ranges are linked to sea spray production mechanisms, consistent with earlier studies [*Grythe et al.*, 2014]. Organics may become more significant in sea-spray in the large accumulation size range or sub- and in-cloud growth of Aitken particles could be enhanced by increased fluxes of DMS associated with high wind speeds [*Lana et al.*, 2011]. However, with the addition of the smaller UHSAS sizes and an order of magnitude growth in number, the correlation disappears. The total aerosol concentration (CN), which additionally includes a larger number of Aitken mode aerosols, has no statistically significant relationship with wind speed.

If wind-speed generation mechanisms are not the source of the bulk of the sub-cloud accumulation mode aerosol (the number between 0.08-0.3 μm), where is it coming from? With the elimination of primary emissions as the source, it is likely the central source of CCN is growth of secondary particles. These may come either from above the boundary layer or within the boundary layer. Based on our previous analysis, Aitken mode production is limited in the boundary layer which suggests they are coming from the free tropospheric Aitken reservoir. If these particles were grown into accumulation mode sizes, they would be a significant source and would have little correlation with wind-speed, as we see in Figure 10. Growth could occur either through in-cloud processing or sub-cloud gas absorption of DMS-oxidation products.

We conclude that it is unlikely that sea-spray aerosols are the primary driver of SO CCN number in summer months. Aerosol composition analysis (3.1.3) supports this as the majority of particles (diameters 0.1-0.5 μm) above, in, and sub-cloud are found to be sulfur-based [*Twohy et al.*, 2020 submitted]. Influences of sea-spray are seen in the sub- and in-cloud particle samples, but they are secondary and often sulfur enriched. The dominant, sulfur-based composition of the particles is consistent with aerosols grown from DMS-oxidation products. Growth of

accumulation mode aerosol from sulfuric acid Aitken mode aerosols, as suggested by our volatility analysis (3.1.3), are very likely a significant contributor to SO CCN in summer. This is consistent with model estimates from *Korhonen et al.* [2008].

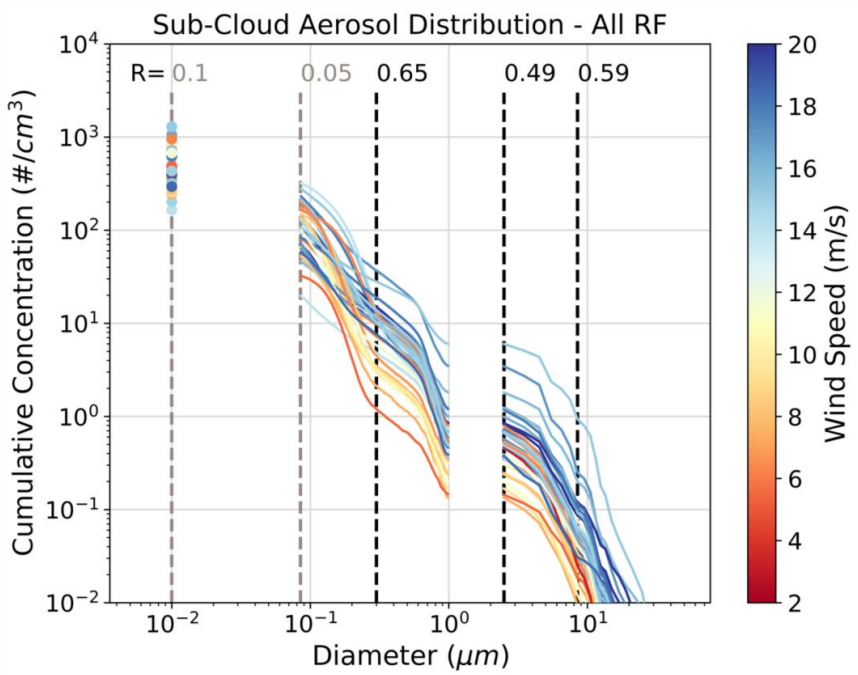

Figure 10 Cumulative size distribution for sub-cloud aerosol sampling colored by wind speed at the aircraft (~150 m). Aerosol number concentrations from CN (dots), UHSAS (accumulation, middle curves), and CDP (coarse, right curves) are screened for cloud and drizzle. Cumulative distribution is summed from the right to the left where CN equals the total number concentration. Correlation coefficients computed between wind speed and the log of the cumulative number concentrations to the right of the dashed lines (gray for not significant and black for significant at 95% confidence) indicate weakening relationship between wind speed and log_{10}(cumulative aerosol number concentration) with a decrease in diameter.

3.2.3 Influence of Aitken Mode Aerosols on Southern Ocean Summertime Cloud Droplet Number Concentrations

Our analysis demonstrates that sulfur-based aerosols have a more significant impact on SO cloud droplet number concentrations than sea-spray particles. Understanding the origin and influence of these sulfur-based aerosols is of primary importance for understanding summertime SO cloud-aerosol interactions. From the pattern of CN, UHSAS, and SA (3.2.1), it is unlikely that these sulfur-based particles are generated from a surface source alone. Instead, free tropospheric Aitken mode particles descending into the boundary layer and growing into accumulation mode sizes could be the missing source of CCN that we observe influencing summertime SO N_d.

Because of the large quantity of Aitken mode aerosol present in the free troposphere, if these particles are an important CCN source they are difficult to deplete. This ability to be replenished has significant implications for SO N_d which is known to have a large precipitation sink of N_d and CCN associated with the mid-latitude storm track. Despite the magnitude of this sink, high SO droplet number concentrations are maintained (N_d ~80-100 cm^{-3}) [*I L McCoy et al.*, 2020 in press]. It is likely that a large and continuous source of aerosol exists in the SO that is able to maintain clouds against persistent collision-coalescence processes that would otherwise rapidly deplete N_d.

We see evidence of a reduction in precipitation depleted cloud and aerosol features in the Southern Ocean relative to a typical sub-tropical marine environment (Figure 9). Both SOCRATES and CSET sampled intermittently precipitating shallow cumulus and stratocumulus clouds: SOCRATES in SO cyclone cold sectors and CSET in the NEP stratocumulus to trade cumulus transition. Similar near-cloud median accumulation mode aerosol concentrations occurred for SOCRATES (~50 cm^{-3}) and CSET (~40 cm^{-3}) when sampling far from continents (Figure 9a). Median N_d is higher and less variable during SOCRATES compared to CSET (~70 to 40 cm^{-3}, Figure 9c). The N_d-UHSAS100 space captures the cloud-aerosol interactions occurring in the NEP and SO and, not too surprisingly, show that in cloud N_d is well correlated with near cloud CCN measured by UHSAS100 in both environments (Figure 9b).

The breadth of the N_d CSET pdf (Figure 9c) is driven by the frequent occurrence of precipitation depleted clouds ($N_d \leq 10$ cm^{-3}) in the cumulus regime west of 140°W. In N_d-UHSAS100 space, these precipitation-depleted cloud features are frequently collocated with depleted CCN (UHSAS100 ≤ 10 cm^{-3}). These features, referred to as "veil" clouds or "ultra-clean" aerosol layers in the literature, occur primarily at the detraining tops of cumulus clouds and are developed through droplet and aerosol number removal by collision-coalescence [*O et al.*, 2018; *Wood et al.*, 2018]. SOCRATES N_d is noticeably missing these precipitation-depleted occurrences despite sampling similar cloud structures (Figure 9).

Why do SO clouds have less precipitation-depleted cloud features? Accumulation mode aerosol is similar in both environments and NEP number concentration encompasses that observed in the SO (Figure 3, Figure 9). However, Aitken mode aerosol concentration is significantly different in these two regimes (sub-cloud median 146 mg^{-1} compared to 380 mg^{-1}, Figure 3). Are free tropospheric Aitken aerosols providing a continuous source for CCN development and thus helping to prevent N_d depletion as a result of persistently drizzling boundary-layer clouds? And if so, how is this N_d-buffering accomplished? We hypothesize one possible mechanism (Figure 11):

I. *Marine biogenic outgassing leads to the generation of widespread high concentrations of small Aitken-mode aerosols in the free troposphere via lifting, scavenging, and cloud outflow nucleation mechanisms (3.1).*

II. *Aitken-mode aerosols make their way into the SO boundary layer through horizontal and vertical advection and turbulent mixing (3.2.1).*

III. *Once in the boundary layer, these small aerosols grow to accumulation mode sizes through in-cloud processing or below-cloud gas absorption (3.2.2).*

IV. *This source of accumulation mode aerosol buffers SO summertime boundary-layer clouds against precipitation-induced depletion of cloud condensation nuclei, resulting in very infrequent occurrences of precipitation-depleted cloud features in SO summertime low clouds. Cloud brightness and longevity are maintained and susceptibility to anthropogenic aerosols is reduced.*

We suggest that the summertime SO is a more aerosol-buffered environment than the summertime NEP, leading to elevated N_d during SOCRATES and a lack of precipitation-depleted features compared to CSET. The evidence presented in this and preceding sections support this mechanism and, more broadly, are strongly suggestive of a more complex cloud-aerosol interaction taking place in the summertime SO than hitherto discussed. However, we acknowledge that more observational analysis and process modeling is required to determine whether high Aitken mode aerosol concentrations are an important driver of SO N_d characteristics. A further assessment of the validity of these steps and the observations still

needed to test this mechanism is presented in the discussion.

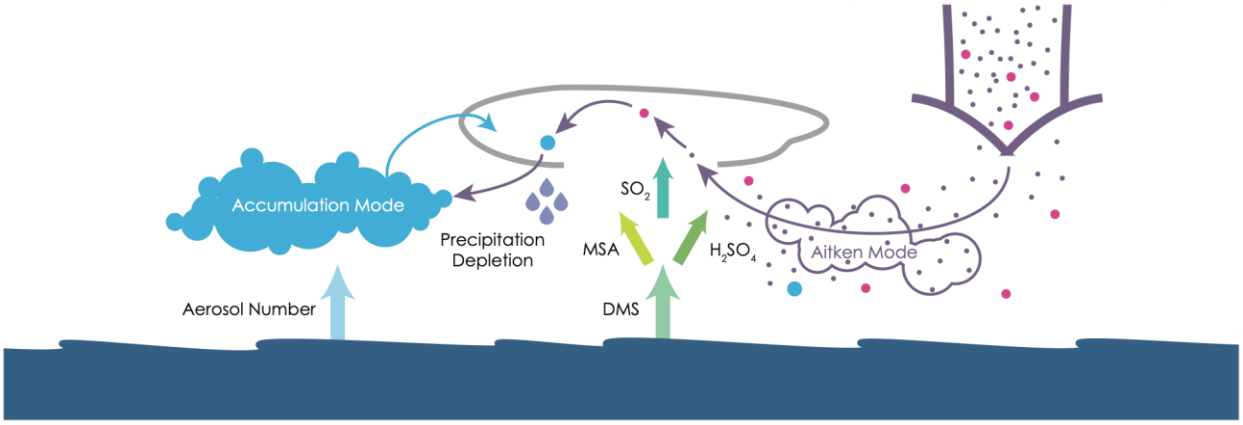

Figure 11 Diagram illustrating hypothetical buffering mechanism for how Aitken mode aerosols influence Southern Ocean clouds and reduce precipitation depletion.

3.2.4 Evaluating Southern Ocean Cloud-Aerosol Interactions in Global Climate Models

Recent satellite comparisons revealed that many state of the art climate models under-predict N_d over the Southern Ocean [*Bodas - Salcedo et al.*, 2019; *I L McCoy et al.*, 2020 in press; *Mulcahy et al.*, 2018; *Revell et al.*, 2019]. Identifying where there are significant inconsistencies between observed and modeled cloud and aerosol characteristics will help in diagnosing the underlying cause of this bias. With this purpose, we compare meteorologically nudged CAM6 hindcasts that use prognostic aerosols and cloud droplet concentrations (2.3) with matched *in situ* observations from the SOCRATES flights. We include an additional model-observation comparison with CSET flights for a sub-tropical baseline of model ability. Testing GCMs using this nudged framework helps us to understand what mechanisms may be contributing to the current N_d bias in models and other discrepancies in cloud-aerosol interactions while ensuring that differences in the large-scale meteorology are small between the simulation and reality.

The Aitken buffering mechanism (3.2.3) is a useful framework for interpreting cloud-aerosol interactions in CAM6 and comparing to observed tendencies. We utilize the N_d-UHSAS100 space previously introduced for observing cloud-aerosol interaction tendencies (Figure 9b) to test cloud responses to adjacent aerosol in CAM6 hindcasts for CSET and SOCRATES (Figure 12c, d). Observations and collocated CAM6 output for each flight during CSET and SOCRATES are binned into 500 m by 2.5° bins (2.1). Comparisons are for bin-matched data where $Z \leq 4$ km, samples are at a distance from continental effects, and both observations and model data are available.

CAM6 consistently underpredicts SOCRATES N_d (model median 23 compared to observed median 70 cm^{-3}, Figure 12e) with little linear correlation to bin matched observations (R=0.26, Figure S6). Surprisingly, the pdf for bin-matched accumulation mode concentrations is very similar to the observations (62 to the observed 52 cm^{-3}, Figure 12b). However, CAM6 poorly captures the observed relationship between N_d and UHSAS100 during SOCRATES (log-log correlation of 0.51 is lower than the observed 0.62) (Figure 12d). This is both due to the low N_d bias and over-produced precipitation-depleted cloud features ($N_d \leq 10$ cm^{-3}) in the model.

CAM6 is closer to observed tendencies during CSET than during SOCRATES. CAM6 N_d is slightly more correlated with observations (R=0.36, Figure S6) and is less biased (30 to

observed 42 cm^{-3}, Figure 12e). As in the SO, CAM6 captures the average observed CSET aerosol concentrations (43 to 34 cm^{-3}, Figure 12a) although it produces a much narrower range of likely concentrations compared to observations. CAM6 captures the majority of the observed CSET N_d-UHSAS relationship (Figure 12c), except for cases with low N_d. The narrower aerosol concentration range may be reducing the correlation of CAM6 relative to the observations (0.54 to 0.71) but the model still performs better than in SOCRATES. While CAM6 produces precipitation-depleted cloud features ($N_d \leq 10$ cm^{-3}), it does not produce these features concurrently with ultra-clean aerosol (UHSAS100 ≤ 10 cm^{-3}).

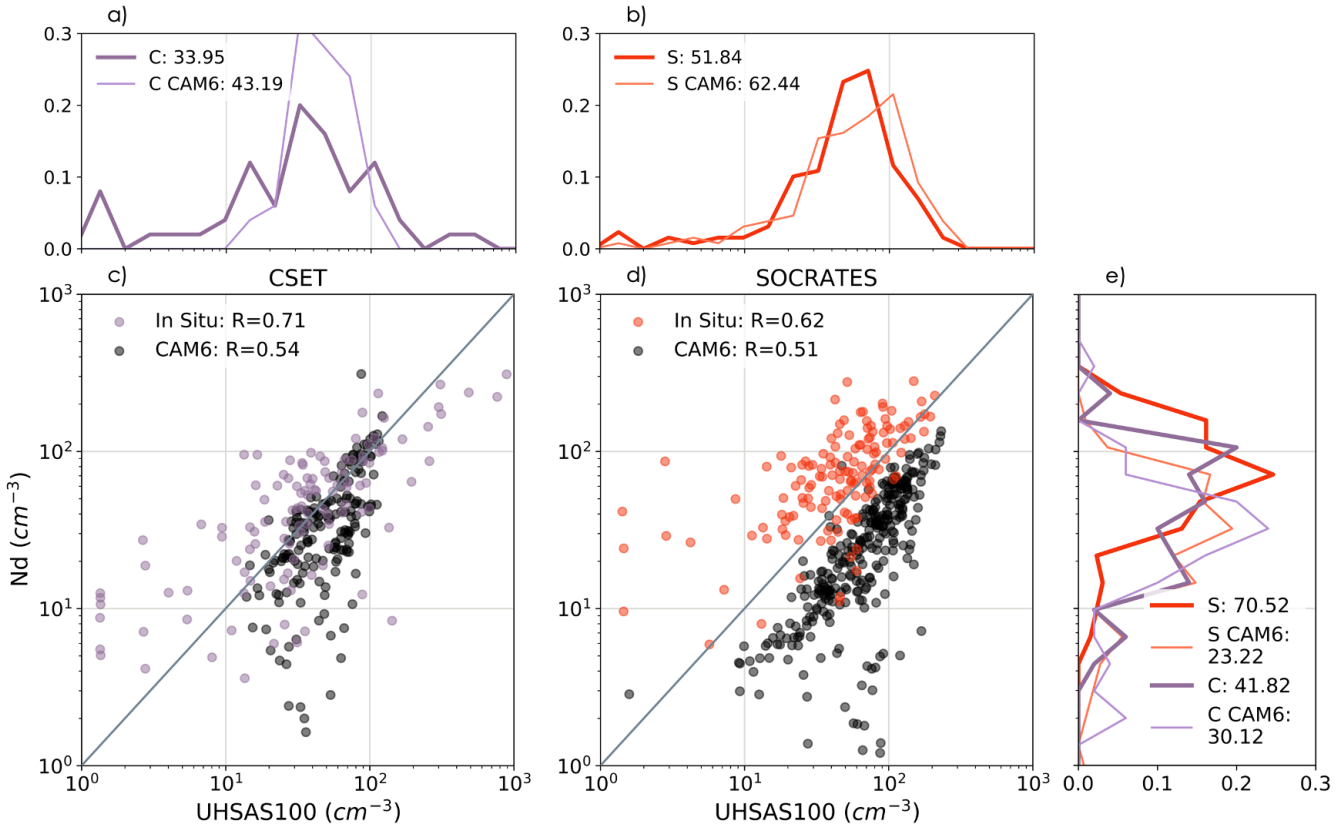

Figure 12 CAM6 (black) and observational (color) comparison for N_d-UHSAS100 relationship from collocated binned composite values for each flight during CSET (c) and SOCRATES (d). Data is taken for $Z \leq 4$ km and in pristine regions: Latitude south of 45°S (SOCRATES) and Longitude' west of 130°W. Corresponding PDFs of aerosol-droplet occurrence for matched binned values occurring for the model and observational data are shown along with median values for UHSAS100 (a, b) and N_d (e).

The better agreement between modeled and observed N_d for CSET compared to SOCRATES suggests that the mechanisms responsible for producing N_d in the SO are likely incomplete in CAM6 and unique to that pristine environment. N_d is developed through a balance of sources and sinks and leads to high and persistent values in the SO [*I L McCoy et al.*, 2020 in press]. The interplay of the mechanisms producing and depleting CCN and thus N_d is complex. The too frequent occurrence of precipitation-depleted N_d in CSET and SOCRATES CAM6 simulations may indicate that precipitation removal processes are too active in the model, as has been seen in other GCMs [*Stephens et al.*, 2010]. This hypothesis is examined for SOCRATES in *Zhou et al.* [2020 submitted] but no consistent tendency in CAM6 precipitation is found connected to low-N_d bias across the campaign. Phase partitioning, particularly production of super-cooled clouds, generally agrees with SOCRATES observations so may not play a large

role in the low N_d bias [*Gettelman et al.*, 2020 submitted; *Zhou et al.*, 2020 submitted]. Activation of CCN into cloud droplets is dependent both on CCN availability and turbulent updrafts. However, there is no consistent turbulent updraft bias in CAM6 across the SOCRATES campaign: CAM6 tends to under-produce turbulence in stable and neutral boundary layers but match turbulence in unstable regimes [*Atlas et al.*, 2020 submitted]. There are noticeable cloud-regime dependent differences in CAM6 precipitation bias as well, with over-production in cumulus-like clouds and under-production in stratocumulus clouds [*Zhou et al.*, 2020 submitted]. Tendencies in precipitation and turbulent updrafts may have competing, regime dependent influences on N_d in CAM6, obscuring the overall impact these biases have on the CAM6 SOCRATES N_d bias.

The largest remaining and uninvestigated contributor to this N_d bias is CCN and its production in CAM6. We have already observed that the number concentrations of CCN are roughly consistent with the observed bin matched aerosol in CSET and SOCRATES (Figure 12a, b). CAM6's simulation of cloud-aerosol interactions in the less biologically active sub-tropics is also more promising as it better resembles the observed relationship and is considerably less biased than in the SO. One possible reason for this is that under-production of biological aerosol, particularly the Aitken aerosols that may be buffering the clouds against precipitation removal, is resulting in an under production of N_d in the SO. In the remainder of this section, we will use our expanded knowledge of the mechanisms impacting aerosol production in the SO to illuminate any discrepancies in modeled aerosol characteristics that may be influencing N_d.

As a first assessment of CAM6's skill in producing aerosol, we compare the observed and simulated number concentrations observed in the subtropics and SO. Extracting total aerosol and CCN (0.6% super-saturation) number concentrations along the flight paths for CSET and SOCRATES, we formulate companion CAM6 altitude pdfs to those in Figure 3 (Figure 13). CAM6 during CSET reproduces the observed aerosol number concentrations for both CN and UHSAS100 with some accuracy, only underestimating the free tropospheric values (Figure 13a, b). CAM6 during SOCRATES reproduces observed aerosol number concentrations in the sub-cloud and above-cloud sampling but only for UHSAS100 (Figure 13a, c, e). The SOCRATES CN simulations for all the altitude pdfs, especially SC and AC, have a severe low-bias compared to observations (Figure 13b, d, and f). The flight matched CAM6 aerosol concentration pdfs for CSET and SOCRATES are strikingly similar despite the large differences in the observational pdfs for these two campaigns. This along with the larger discrepancy with observed CN during SOCRATES suggests that CAM6 may be missing mechanisms specific to the more biologically active summertime SO that are key in generating Aitken aerosols.

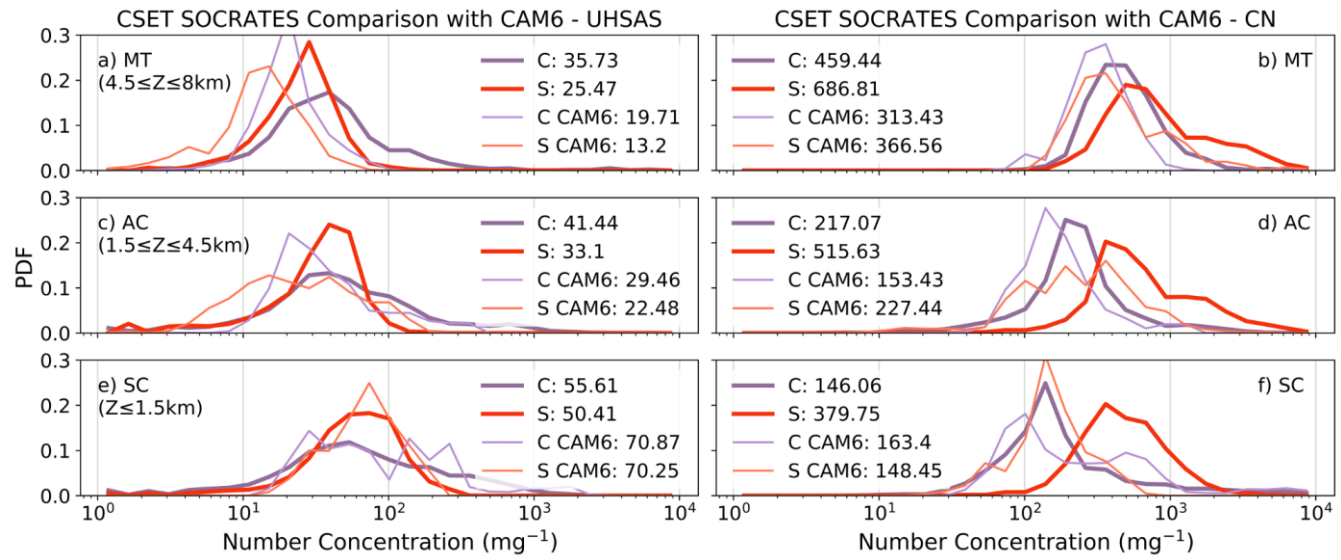

Figure 13 As in Figure 3 but including CAM6 aerosol concentrations extracted along the flight tracks.

While the modeled accumulation number concentrations are consistent with observations during both CSET and SOCRATES, it is possible that this is due more to an imbalance in sea-spray production rather than an accurate depiction of all aerosol in these environments. Recent analysis of the HadGEM3 model found an overly active sea spray-wind speed mechanism which produced too much CCN [*Revell et al.*, 2019]. An examination of aerosol composition and the relationship between wind speed and number concentration suggests a similar problem may exist with CAM6. The MAM4 aerosol scheme produces four modes of aerosol: accumulation, Aitken, coarse, and insoluble coarse. Aerosol size is the same for all aerosols in each mode and mixing ratios are used to denote composition. To understand the relative contribution of aerosol type, we examine the magnitudes of the aerosol constituent mixing ratios for each mode. Representative mean vertical profiles of number concentration and composition mixing ratio are calculated for each mode and each flight along with a campaign average profile for SOCRATES and CSET (Figure S7, Figure S8). Sub-cloud ($Z \leq 1500$ m) coarse and accumulation mode aerosol mixing ratios are dominated by sea salt in the SO (Figure S7a). Sulfate (SO_4) is the secondary contributor to accumulation mode and dominates Aitken mode in the SO (Figure S7a, b). However, the sub-tropics see an equal contribution in accumulation mode between sea salt and sulfate (Figure S8a). Coarse mode is still driven by sea salt and Aitken by SO_4 in CSET (Figure S8b, c).

We would expect that if sea-spray is overproduced in CAM6 then it would dominate in an environment with higher wind speeds, such as the SO (e.g. Figure S7a). However, observationally we have evidence that the sub-cloud and in-cloud aerosols are not dominated by sea-spray (3.1.3). We can additionally test the nature of aerosol production in CAM6 by comparing, as we did in 3.2.2, the log of the number concentration with the wind speed. In an approximate analog of the cumulative correlation coefficients in Figure 10, we correlate $\log_{10}$ number concentration and wind speed near the surface ($Z \leq 500$ m) for total number ($R=0.01$, not significant at 95%), accumulation and coarse ($R=0.16$, significant), and coarse mode ($R= 0.42$, significant) aerosols. In contrast to the SOCRATES observations where only coarse mode aerosol was significantly correlated with wind speed, both coarse and accumulation mode number concentrations are significantly correlated with wind speed in CAM6.

Ultimately, aerosol enabled GCMs need to be able to capture the differences in N_d between the sub-tropics and the biologically active SO in order to accurately simulate the radiative impacts of clouds in these regions. Producing an observationally consistent number concentration for CCN but from an incorrect aerosol production pathway may lead to a masking of other biases that subsequently influence N_d. In particular, over-producing sea salt and under-producing sulfate in the SO could explain why there are larger discrepancies observed in SOCRATES N_d than in the less biologically active sub-tropics (Figure 9). We have also shown that CAM6 has difficulty in producing enough Aitken particles (Figure 13b, d, and f). Because this is a biologically dominated mode (Figure S7), it is likely that this under-production is linked to insufficient DMS production, distribution, or oxidation into viable pre-cursor gases for particle formation. A simple comparison between the roughly equal January and February mid-tropospheric sampling during SOCRATES indicates that while observational pdfs of CN are consistent between the two months, CAM6 Aitken mode is hugely different (Figure S9). This is likely linked to the discrete DMS climatology used in CAM6 which decreases sharply from January to February [*Lana et al.*, 2011]. Note that even though January is closer to the observed pdf, CAM6 still under-produces the high CN concentrations that we link to RPF. While there are some immediate fixes that can be used to improve simulated biological activity and sources important for aerosol production (e.g. developing a higher time resolution climatology or an interactive DMS production model), the mechanisms controlling how and where aerosol is produced and grown to CCN are likely incomplete or missing in CAM6. This paper illustrates some of the complexities of these production and growth mechanisms and underlines the importance of understanding and capturing these mechanisms in GCMs in order to advance the simulation of SO cloud-aerosol interactions and thereby reduce SO radiative biases.

4 Summary and Discussion

We present evidence of widespread and frequent recent particle formation (RPF) in the summertime Southern Ocean free troposphere. Signatures of free tropospheric RPF observed during *in situ* airborne sampling from the SOCRATES field campaign included: high concentrations of total aerosol number concentrations (CN> 1000 mg^{-1}) typically accompanied by large and rapid spatial CN variability, low accumulation and coarse mode aerosol surface area (<10 μm^2 mg^{-1}), and small accumulation-mode aerosol concentrations (UHSAS100 < 80 mg^{-1}). These primarily Aitken mode particles volatilized when heated to ~60°C, suggesting they are composed from sulfuric acid or an even more volatile DMS-oxidation product. Back-trajectory analysis of SOCRATES sampled air masses revealed RPF classified events (CN ≥ 2500 mg^{-1}) recently underwent ascent from below 1 km to free-tropospheric altitudes. Ascent was driven by diverse synoptic mechanisms across the campaign but primarily was associated with uplift through warm-conveyor belts or sub-polar vortices.

Our results provide evidence supporting a hypothesized particle production mechanism: boundary-layer air parcels rich in marine biogenic gases (i.e. DMS) are swept up into stratiform clouds, precipitation scavenges large aerosols from the air parcel and reduces aerosol surface area, DMS oxidizes into precursor gases (e.g. SO_2, H_2SO_4, and MSA) upon the air parcel exiting the cloud, and gas to particle conversion is enabled in the free troposphere. This newly identified synoptic mechanism is a variant on other cloud-outflow associated particle formation [*Kerminen et al.*, 2018]. Specifically, in the SO, this mechanism acts in addition to the particle formation generated in outflow from overshooting cumulus congestus clouds [*Clarke et al.*, 1998]. Synoptic scale ascent over the SO is deeper and more widespread than cumulus outflow and

helps explain the high Aitken mode concentrations observed frequently throughout the SO summertime free troposphere. Both mechanisms assume outgassing of DMS from a biologically active ocean and are expected to operate much more frequently in summer than in winter.

Aitken-mode aerosol concentrations are nearly as high in the SO boundary layer as in the free troposphere. They are substantially higher than those typically measured in and above cloudy boundary layers over remote parts of the marine subtropics. We find a negligible relationship between sub-cloud wind speed and aerosol concentrations for both Aitken and accumulation mode sizes, suggesting that sea spray aerosol does not control CCN number over the summertime SO. Sea-spray is likely more important for large aerosols, as exhibited by stronger correlations between wind speed and large accumulation and coarse mode sizes. STEM analysis [*Twohy et al.*, 2020 submitted] shows above, in, and sub-cloud particle (0.1-0.5 μm) compositions are dominantly sulfur-based. We conclude that sea-spray particles are of secondary importance to sulfur-based particles in controlling the CCN budget and influencing summertime SO cloud droplet number concentrations.

The missing source of sub-cloud, sulfur-based particles maintaining CCN in the SO may be the reservoir of free tropospheric Aitken mode aerosol. Previous work has demonstrated descent of free tropospheric Aitken particles into the boundary layer is possible [*Covert et al.*, 1996; *Humphries et al.*, 2016] and that this is an important CCN source in the NEA [*Sanchez et al.*, 2018; *Zheng et al.*, 2018]. A global chemical transport model showed entrainment of free tropospheric H_2SO_4 particles into the MBL may be the dominant mechanism for DMS influence on CCN and that these FT Aitken particles are the dominant contributor to CCN in the SH summertime oceans [*Korhonen et al.*, 2008]. Droplet number concentrations are consistently high in the SO and the occurrence of precipitation depleted cloud features are infrequent. This leads us to hypothesize that the summertime SO is a buffered system in which there are copious small aerosol particles that are inefficiently scavenged by precipitation but can nucleate into droplets under suitable conditions, sustaining the droplet concentration of SO clouds against precipitation removal processes. Evidence supporting our hypothesized buffering mechanism is presented along with a contrasting sub-tropical analysis to understand the significance of SO cloud-aerosol behavior.

Our hypothesized aerosol lifecycle would involve large spatial scales as it requires lofting of DMS, production of Aitken mode aerosols in the free troposphere from DMS-oxidation products, Aitken particle descent into the boundary layer, and Aitken particle growth into accumulation mode sizes below cloud. This is consistent with stronger correlations found between DMS fluxes and droplet number concentration over large spatial scales [*Andreae et al.*, 1995; *Covert et al.*, 1996; *D T McCoy et al.*, 2015] and limited local correlations [*Covert et al.*, 1996].

In this study, we utilize the buffering mechanism as a framework for interpreting cloud-aerosol interactions in nudged simulations from CAM6. Despite capturing cloud-aerosol interactions in the sub-tropics, we find a persistent low-bias in SO N_d relative to SOCRATES observations. This regional discrepancy and our preliminary aerosol composition investigations suggest that i) biological aerosol is under-produced in CAM6 and ii) that it is likely there is a compensating bias of sea-spray over-production as has been seen in other GCMs [*Revell et al.*, 2019]. Despite capturing the magnitude of SO CCN number, the composition of these aerosols is significantly different from the biologically dominated aerosols observed during SOCRATES. CAM6 exhibits systematically low numbers of CN that, in better keeping with observations, are primarily sulfur-based. These two inconsistencies suggest that the low CAM6 N_d exhibited

across the campaign may be connected with an underproduction of biological aerosol. Further, our results suggest that CAM6 may have incomplete or missing radiatively-important aerosol production and growth mechanisms associated with biological aerosol, something other state of the art GCMs suffer from in the Southern Ocean [*Bodas - Salcedo et al.*, 2019; *I L McCoy et al.*, 2020 in press; *Revell et al.*, 2019]. Both mechanisms introduced in this text (i.e. particle production through synoptic-uplift and aerosol buffering against precipitation depletion) are potential candidates for improving CAM6 representation of biologically driven aerosol-cloud interactions. Neglecting natural new particle formation in GCMs will lead to an underestimation of the strength of the radiative forcing associated with aerosol-cloud interactions [*Gordon et al.*, 2017], further supporting the importance of understanding and capturing these mechanisms.

The proposed buffering mechanism and its influence on SO and other pristine environments needs more in-depth investigation. LES simulations and additional observations of the SO aerosol-cloud system will be important in assessing mechanism robustness. One important aspect that has not been addressed here but could be examined though LES simulations of the SO environment is the time scale over which these processes occur. The feasibility of free tropospheric Aitken particles buffering the CCN budget will be determined by the balance between the rate of SO N_d depletion by precipitation compared to the rate of Aitken mode particle growth to cloud affecting sizes. Examining the role of mixed-phase and super-cooled cloud physics on aerosol cloud interactions in the SO should be considered as well for a complete understanding of this mechanism and its generalizability to other pristine environments. The influence of the buffering mechanism may differ across regions, a key consideration in understanding how pristine clouds respond to anthropogenic aerosol [*Carslaw et al.*, 2013] and in constraining radiative forcing associated with cloud-aerosol interactions [*Bellouin*, 2019].

Additional observations from the Southern Ocean can help us understand the influence of the synoptic particle production mechanism and the validity of the buffering hypothesis. We know that small particles may be playing an important role in the SO, thus it is critical to sample a size distribution that includes the Aitken and nucleation mode ranges and understand its evolution with altitude, geography, and near clouds. Aerosol composition and trace gas species measured concurrently with this size distribution will reveal the origins of the aerosols important to the CCN budget. Knowledge of the particle composition as well as the availability of DMS and pre-cursor gases in the Southern Ocean at the surface and aloft would enable rate calculations and estimates of processing time for aerosol formation, growth, and depletion. Such estimates would help determine how phytoplankton and their DMS emissions exert long-range influence on clouds and aerosols in the Southern Ocean. New particle production is expected to be seasonal due to its biological dependence. Repeating the same statistical sampling methodology from SOCRATES in a shoulder season (i.e. austral spring or fall) will help us to understand the degree of fluctuation in the aerosol budget with biological activity and the subsequent influence on N_d. Seasonal examinations of cloud and aerosol characteristics as well as characterization of pristine aerosol sources and sinks will further help to correct current GCM discrepancies [*Bodas - Salcedo et al.*, 2019; *I L McCoy et al.*, 2020 in press].

Before beginning a separate investigation of the Southern Ocean, however, we suggest that pre-existing datasets from flight, ship, satellite, and ground stations should be leveraged to their fullest extent to determine the ubiquity of the buffering mechanism and the role that it plays in modulating cloud-aerosol interactions across the globe. Measurements of other pristine regions of the world can help us to understand the uniqueness of the SO as well as the role of the

buffering mechanism in controlling cloud susceptibility in diverse environments. Determining the degree of susceptibility in pristine environments will have important implications for the pre-industrial state and constraining the radiative effect of aerosol-cloud interactions under industrialization.

Acknowledgments, Samples, and Data

The authors wish to thank Mike Reeves for help in interpreting aerosol observations. They further thank Rachel Atlas, Xiaoli Zhou, Matt Wyant, Cristina McCluskey, Kevin Sanchez, and the SOCRATES team for productive discussions of this work.

The National Science Foundation supports the SOCRATES campaign and its continued research efforts (AGS-1660609). Additionally, CHT acknowledges funding through grant AGS-1660605.

ILM, CSB, and RW developed scientific hypothesis, method of approach, and wrote the paper. ILM obtained and analyzed data, ran HYSPLIT trajectories, and extracted model data to match observations. CHT and DWT helped to interpret volatility estimates. AG and CB supplied CAM6 nudged simulations for CSET and SOCRATES. All authors contributed to writing and editing the paper.

NCAR EOL provided aircraft data from the SOCRATES campaign [*Laboratory*, 2019] and CSET campaign [*Laboratory*, 2017]. All information and datasets can be found through the supporting EOL websites (https://www.eol.ucar.edu/field_projects/socrates and http://catalog.eol.ucar.edu/cset). HYSPLIT Back Trajectories were calculated from SOCRATES positions using the publicly available HYSPLIT code (https://www.ready.noaa.gov/HYSPLIT.php). ERA5 Reanalysis products can be ordered through the online database at ECMWF (https://www.ecmwf.int/en/forecasts/datasets/reanalysis-datasets/era5). CAM6 Simulations for SOCRATES and CSET are archived at the NCAR Earth System Grid (DOI forthcoming).

References

Ahn, E., Y. Huang, S. T. Siems, and M. J. Manton (2018), A Comparison of Cloud Microphysical Properties Derived From MODIS and CALIPSO With In Situ Measurements Over the Wintertime Southern Ocean, *Journal of Geophysical Research: Atmospheres*, *123*(19), 11,120-111,140, doi:10.1029/2018jd028535.

Albrecht, B. A., et al. (2019), Cloud System Evolution in the Trades (CSET): Following the Evolution of Boundary Layer Cloud Systems with the NSF–NCAR GV, *Bulletin of the American Meteorological Society*, *100*(1), 93-121, doi:10.1175/bams-d-17-0180.1.

Andreae, M. O., W. Elbert, and S. J. Demora (1995), Biogenic Sulfur Emissions and Aerosols over the Tropical South-Atlantic .3. Atmospheric Dimethylsulfide, Aerosols and Cloud Condensation Nuclei, *Journal of Geophysical Research-Atmospheres*, *100*(D6), 11335-11356, doi:Doi 10.1029/94jd02828.

Andreae, M. O., C. D. Jones, and P. M. Cox (2005), Strong present-day aerosol cooling implies a hot future, *Nature*, *435*(7046), 1187-1190, doi:10.1038/nature03671.

Atlas, R. L., C. S. Bretherton, P. N. Blossey, A. Gettelman, C. Bardeen, P. Lin, and Y. Ming (2020 submitted), How well do large-eddy simulations and global climate models represent observed boundary layer structures and low clouds over the summertime Southern Ocean?, *J. Adv. Model. Earth Syst.*

1123 Ayers, G. P., J. M. Cainey, R. W. Gillett, and J. P. Ivey (1997), Atmospheric sulphur and cloud condensation nuclei
1124 in marine air in the Southern Hemisphere, *Philosophical Transactions of the Royal Society of London Series B-*
1125 *Biological Sciences*, *352*(1350), 203-211.

1126 Ayers, G. P., and R. W. Gillett (2000), DMS and its oxidation products in the remote marine atmosphere:
1127 implications for climate and atmospheric chemistry, *Journal of Sea Research*, *43*(3), 275-286,
1128 doi:https://doi.org/10.1016/S1385-1101(00)00022-8.

1129 Ayers, G. P., and J. L. Gras (1991), Seasonal relationship between cloud condensation nuclei and aerosol
1130 methanesulphonate in marine air, *Nature*, *353*(6347), 834-835, doi:10.1038/353834a0.

1131 Bellouin, N., Quaas, J., Gryspeerdt, E., Kinne, S., Stier, P., Watson-Parris, D., Boucher, O., Carslaw, K. S.,
1132 Christensen, M., Daniau, A.-L., Dufresne, J.-L., Feingold, G., Fiedler, S., Forster, P., Gettelman, A., Haywood, J.M.,
1133 Lohmann, U., Malavelle, F., Mauritsen, T., McCoy, D.T., Myhre, G., Muelmenstaedt, J., Neubauer, D., Possner, A.,
1134 Rugenstein, M., Sato, Y., Schulz, M., Schwartz, S.E., Sourdeval, O., Storelvmo, T., Toll, V., Winker, D. and
1135 Stevens, B. (2019), Bounding global aerosol radiative forcing of climate change, *Reviews of Geophysics*.

1136 Berresheim, H. (2002), Gas-aerosol relationships of H2SO4, MSA, and OH: Observations in the coastal marine
1137 boundary layer at Mace Head, Ireland, *Journal of Geophysical Research*, *107*(D19), doi:10.1029/2000jd000229.

1138 Bigg, E. K. (2007), Sources, nature and influence on climate of marine airborne particles, *Environmental Chemistry*,
1139 *4*(3), 155-161, doi:10.1071/en07001.

1140 Bigg, E. K., and C. Leck (2008), The composition of fragments of bubbles bursting at the ocean surface, *Journal of*
1141 *Geophysical Research-Atmospheres*, *113*(D11), doi:10.1029/2007jd009078.

1142 Bodas-Salcedo, A., P. G. Hill, K. Furtado, K. D. Williams, P. R. Field, J. C. Manners, and P. Hyder (2016), Large
1143 Contribution of Supercooled Liquid Clouds to the Solar Radiation Budget of the Southern Ocean, *Journal of*
1144 *Climate*, *29*(11), 4213-4228, doi:10.1175/jcli-d-15-0564.1.

1145 Bodas-Salcedo, A., K. D. Williams, P. R. Field, and A. P. Lock (2012), The Surface Downwelling Solar Radiation
1146 Surplus over the Southern Ocean in the Met Office Model: The Role of Midlatitude Cyclone Clouds, *Journal of*
1147 *Climate*, *25*(21), 7467-7486, doi:10.1175/jcli-d-11-00702.1.

1148 Bodas-Salcedo, A., K. D. Williams, M. A. Ringer, I. Beau, J. N. S. Cole, J. L. Dufresne, T. Koshiro, B. Stevens, Z.
1149 Wang, and T. Yokohata (2014), Origins of the Solar Radiation Biases over the Southern Ocean in CFMIP2 Models,
1150 *Journal of Climate*, *27*(1), 41-56, doi:10.1175/jcli-d-13-00169.1.

1151 Bodas-Salcedo, A., J. P. Mulcahy, T. Andrews, K. D. Williams, M. A. Ringer, P. R. Field, and G. S. Elsaesser
1152 (2019), Strong dependence of atmospheric feedbacks on mixed-phase microphysics and aerosol-cloud interactions in
1153 HadGEM3, *J. Adv. Model. Earth Syst.*, *11*(6), 1735-1758, doi:10.1029/2019ms001688.

1154 Boers, R., J. B. Jensen, and P. B. Krummel (1998), Microphysical and short-wave radiative structure of
1155 stratocumulus clouds over the Southern Ocean: Summer results and seasonal differences, *Quarterly Journal of the*
1156 *Royal Meteorological Society*, *124*(545), 151-168, doi:10.1002/qj.49712454507.

1157 Bretherton, C. S., I. L. McCoy, J. Mohrmann, R. Wood, V. Ghate, A. Gettelman, C. G. Bardeen, B. A. Albrecht, and
1158 P. Zuidema (2019), Cloud, Aerosol, and Boundary Layer Structure across the Northeast Pacific Stratocumulus-
1159 Cumulus Transition as Observed during CSET, *Monthly Weather Review*, *147*(6), 2083-2103, doi:10.1175/Mwr-D-
1160 18-0281.1.

1161 Carslaw, K. S., et al. (2013), Large contribution of natural aerosols to uncertainty in indirect forcing, *Nature*,
1162 *503*(7474), 67-+, doi:10.1038/nature12674.

1163 Catto, J. L., E. Madonna, H. Joos, I. Rudeva, and I. Simmonds (2015), Global Relationship between Fronts and
1164 Warm Conveyor Belts and the Impact on Extreme Precipitation, *Journal of Climate*, *28*(21), 8411-8429,
1165 doi:10.1175/Jcli-D-15-0171.1.

1166 Chand, D., R. Wood, S. J. Ghan, M. Wang, M. Ovchinnikov, P. J. Rasch, S. Miller, B. Schichtel, and T. Moore
1167 (2012), Aerosol optical depth increase in partly cloudy conditions, *Journal of Geophysical Research: Atmospheres*,
1168 *117*(D17), n/a-n/a, doi:10.1029/2012jd017894.

1169 Charlson, R. J., J. E. Lovelock, M. O. Andreae, and S. G. Warren (1987), Oceanic Phytoplankton, Atmospheric
1170 Sulfur, Cloud Albedo and Climate, *Nature*, *326*(6114), 655-661, doi:DOI 10.1038/326655a0.

1171 Clarke, A. D. (1991), A thermo-optic technique for in situ analysis of size-resolved aerosol physicochemistry,
1172 *Atmospheric Environment. Part A. General Topics*, *25*(3), 635-644, doi:https://doi.org/10.1016/0960-
1173 1686(91)90061-B.

1174 Clarke, A. D. (1993), Atmospheric nuclei in the Pacific midtroposphere: Their nature, concentration, and evolution,
1175 *Journal of Geophysical Research: Atmospheres*, *98*(D11), 20633-20647, doi:10.1029/93jd00797.

1176 Clarke, A. D., J. L. Varner, F. Eisele, R. L. Mauldin, D. Tanner, and M. Litchy (1998), Particle production in the
1177 remote marine atmosphere: Cloud outflow and subsidence during ACE 1, *Journal of Geophysical Research-*
1178 *Atmospheres*, *103*(D13), 16397-16409, doi:10.1029/97jd02987.

1179 Clement, C. F., I. J. Ford, C. H. Twohy, A. Weinheimer, and T. Campos (2002), Particle production in the outflow
1180 of a midlatitude storm, *Journal of Geophysical Research: Atmospheres*, *107*(D21), AAC 5-1-AAC 5-9,
1181 doi:10.1029/2001jd001352.

1182 Covert, D. S., V. N. Kapustin, T. S. Bates, and P. K. Quinn (1996), Physical properties of marine boundary layer
1183 aerosol particles of the mid-Pacific in relation to sources and meteorological transport, *101*(D3), 6919-6930,
1184 doi:doi:10.1029/95JD03068.

1185 Eckhardt, S., A. Stohl, H. Wernli, P. James, C. Forster, and N. Spichtinger (2004), A 15-Year Climatology of Warm
1186 Conveyor Belts, *Journal of Climate*, *17*(1), 218-237, doi:10.1175/1520-0442(2004)017<0218:Aycowc>2.0.Co;2.

1187 Fitzgerald, J. W. (1991), Marine aerosols: A review, *Atmospheric Environment. Part A. General Topics*, *25*(3), 533-
1188 545, doi:https://doi.org/10.1016/0960-1686(91)90050-H.

1189 Forster, P. M. (2016), Inference of Climate Sensitivity from Analysis of Earth's Energy Budget, *Annual Review of*
1190 *Earth and Planetary Sciences*, *44*(1), 85-106, doi:10.1146/annurev-earth-060614-105156.

1191 Fossum, K. N., et al. (2018), Summertime Primary and Secondary Contributions to Southern Ocean Cloud
1192 Condensation Nuclei, *Sci Rep*, *8*(1), 13844, doi:10.1038/s41598-018-32047-4.

1193 Gelaro, R., et al. (2017), The Modern-Era Retrospective Analysis for Research and Applications, Version 2
1194 (MERRA-2), *Journal of Climate*, *30*(14), 5419-5454, doi:10.1175/jcli-d-16-0758.1.

1195 Gettelman, A., C. G. Bardeen, C. S. McCluskey, E. J□arvinen, J. Stith, C. Bretherton, G. McFarquhar, C. Twohy, J.
1196 D'Alessandro, and W. Wu (2020 submitted), Simulating Observations of Southern Ocean Clouds and Implications
1197 for Climate, *Journal of Geophysical Research: Atmospheres*.

1198 Gordon, H., et al. (2017), Causes and importance of new particle formation in the present-day and preindustrial
1199 atmospheres, *Journal of Geophysical Research: Atmospheres*, *122*(16), 8739-8760, doi:10.1002/2017jd026844.

1200 Grosvenor, D. P., et al. (2018), Remote Sensing of Droplet Number Concentration in Warm Clouds: A Review of
1201 the Current State of Knowledge and Perspectives, *Rev Geophys*, *56*(2), 409-453, doi:10.1029/2017RG000593.

1202 Grythe, H., J. Ström, R. Krejci, P. Quinn, and A. Stohl (2014), A review of sea-spray aerosol source functions using
1203 a large global set of sea salt aerosol concentration measurements, *Atmospheric Chemistry and Physics*, *14*(3), 1277-
1204 1297, doi:10.5194/acp-14-1277-2014.

1205 Hakim, J. R. H. G. J. (2013), *An Introduction to Dynamic Meteorology*, Fifth ed., Elseveir, Academic Press,
1206 doi:https://doi.org/10.1016/C2009-0-63394-8.

1207 Hamilton, D. S., L. A. Lee, K. J. Pringle, C. L. Reddington, D. V. Spracklen, and K. S. Carslaw (2014), Occurrence
1208 of pristine aerosol environments on a polluted planet, *Proceedings of the National Academy of Sciences of the*
1209 *United States of America*, *111*(52), 18466-18471, doi:10.1073/pnas.1415440111.

1210 Hobbs, P. V. (1971), Simultaneous Airborne Measurements of Cloud Condensation Nuclei and Sodium-Containing
1211 Particles over Ocean, *Quarterly Journal of the Royal Meteorological Society*, *97*(413), 263-&, doi:DOI
1212 10.1256/smsqj.41301.

1213 Humphries, R. S., A. R. Klekociuk, R. Schofield, M. Keywood, J. Ward, and S. R. Wilson (2016), Unexpectedly
1214 high ultrafine aerosol concentrations above East Antarctic sea ice, *Atmospheric Chemistry and Physics*, *16*(4), 2185-
1215 2206, doi:10.5194/acp-16-2185-2016.

1216 Kazil, J., H. Wang, G. Feingold, A. D. Clarke, J. R. Snider, and A. R. Bandy (2011), Modeling chemical and aerosol
1217 processes in the transition from closed to open cells during VOCALS-REx, *Atmospheric Chemistry and Physics*,
1218 *11*(15), 7491-7514, doi:10.5194/acp-11-7491-2011.

1219 Kerminen, V.-M., X. Chen, V. Vakkari, T. Petäjä, M. Kulmala, and F. Bianchi (2018), Atmospheric new particle
1220 formation and growth: review of field observations, *Environmental Research Letters*, *13*(10), doi:10.1088/1748-
1221 9326/aadf3c.

1222 Korhonen, H., K. S. Carslaw, D. V. Spracklen, G. W. Mann, and M. T. Woodhouse (2008), Influence of oceanic
1223 dimethyl sulfide emissions on cloud condensation nuclei concentrations and seasonality over the remote Southern
1224 Hemisphere oceans: A global model study, *Journal of Geophysical Research-Atmospheres*, *113*(D15),
1225 doi:10.1029/2007jd009718.

1226 Kupc, A., C. Williamson, N. L. Wagner, M. Richardson, and C. A. Brock (2018), Modification, calibration, and
1227 performance of the Ultra-High Sensitivity Aerosol Spectrometer for particle size distribution and volatility
1228 measurements during the Atmospheric Tomography Mission (ATom) airborne campaign, *Atmospheric*
1229 *Measurement Techniques*, *11*(1), 369-383, doi:10.5194/amt-11-369-2018.

1230 Laboratory, U. N.-E. O. (2017), Low Rate (LRT - 1 sps) Navigation, State Parameter, and Microphysics Flight-
1231 Level Data, edited, doi:https://doi.org/10.5065/D65Q4T96.

1232 Laboratory, U. N.-E. O. (2019), Low Rate (LRT - 1 sps) Navigation, State Parameter, and Microphysics Flight-
1233 Level Data, edited, doi: https://doi.org/10.5065/D6M32TM9

1234 Lana, A., et al. (2011), An updated climatology of surface dimethlysulfide concentrations and emission fluxes in the
1235 global ocean, *Global Biogeochemical Cycles*, *25*(1), n/a-n/a, doi:10.1029/2010gb003850.

1236 Liu, X., P. L. Ma, H. Wang, S. Tilmes, B. Singh, R. C. Easter, S. J. Ghan, and P. J. Rasch (2016), Description and
1237 evaluation of a new four-mode version of the Modal Aerosol Module (MAM4) within version 5.3 of the Community
1238 Atmosphere Model, *Geoscientific Model Development*, *9*(2), 505-522, doi:10.5194/gmd-9-505-2016.

1239 Mauldin, R. L., D. J. Tanner, J. A. Heath, B. J. Huebert, and F. L. Eisele (1999), Observations of H2SO4and MSA
1240 during PEM-Tropics-A, *Journal of Geophysical Research: Atmospheres*, *104*(D5), 5801-5816,
1241 doi:10.1029/98jd02612.

McCoy, D. T., S. M. Burrows, R. Wood, D. P. Grosvenor, S. M. Elliott, P.-L. Ma, P. J. Rasch, and D. L. Hartmann (2015), Natural aerosols explain seasonal and spatial patterns of Southern Ocean cloud albedo, *Science Advances*, *1*(6), doi:10.1126/sciadv.1500157.

McCoy, I. L., et al. (2020 in press), The hemispheric contrast in cloud microphysical properties constrains aerosol forcing, *Proc Natl Acad Sci U S A*, doi:10.1073/pnas.1922502117.

McFarquhar, G., et al. (2020 submitted), Observations of clouds, aerosols, precipitation, and surface radiation over the Southern Ocean: An overview of CAPRICORN, MARCUS, MICRE and SOCRATES, *Bull. Amer. Meteorol. Soc.*

Mulcahy, J. P., et al. (2018), Improved Aerosol Processes and Effective Radiative Forcing in HadGEM3 and UKESM1, *J. Adv. Model. Earth Syst.*, *10*(11), 2786-2805, doi:10.1029/2018ms001464.

Noone, K. J., J. A. Ogren, J. Heintzenberg, R. J. Charlson, and D. S. Covert (1988), Design and Calibration of a Counterflow Virtual Impactor for Sampling of Atmospheric Fog and Cloud Droplets, *Aerosol Science and Technology*, *8*(3), 235-244, doi:10.1080/02786828808959186.

O, K.-T., R. Wood, and C. S. Bretherton (2018), Ultraclean Layers and Optically Thin Clouds in the Stratocumulus-to-Cumulus Transition. Part II: Depletion of Cloud Droplets and Cloud Condensation Nuclei through Collision-Coalescence, *Journal of the Atmospheric Sciences*, *75*(5), 1653-1673, doi:10.1175/Jas-D-17-0218.1.

O'Dowd, C. D., J. A. Lowe, M. H. Smith, B. Davison, N. Hewitt, and R. M. Harrison (1997), Biogenic sulphur emissions and inferred non-sea-salt-sulphate cloud condensation nuclei in and around Antarctica, *Journal of Geophysical Research-Atmospheres*, *102*(11D), 12839-12854, doi:10.1029/96jd02749.

Orsini, D. A., A. Wiedensohler, F. Stratmann, and D. S. Covert (1999), A New Volatility Tandem Differential Mobility Analyzer to Measure the Volatile Sulfuric Acid Aerosol Fraction, *Journal of Atmospheric and Oceanic Technology*, *16*(6), 760-772, doi:10.1175/1520-0426(1999)016<0760:Anvtdm>2.0.Co;2.

Revell, L. E., et al. (2019), The sensitivity of Southern Ocean aerosols and cloud microphysics to sea spray and sulfate aerosol production in the HadGEM3-GA7.1 chemistry–climate model, *Atmos. Chem. Phys.*, *19*(24), 15447-15466, doi:10.5194/acp-19-15447-2019.

Sanchez, K. J., et al. (2018), Substantial Seasonal Contribution of Observed Biogenic Sulfate Particles to Cloud Condensation Nuclei, *Sci Rep*, *8*(1), 3235, doi:10.1038/s41598-018-21590-9.

Schmid, O., B. Eimer, D. E. Hagen, and P. D. Whitefield (2002), Investigation of Volatility Method for Measuring Aqueous Sulfuric Acid on Mixed Aerosols, *Aerosol Science and Technology*, *36*(8), 877-889, doi:10.1080/02786820290038519.

Seinfeld, J. H., and S. N. Pandis (2006), *Atmospheric chemistry and physics from air pollution to climate change*, Second edition. ed., Hoboken, New Jersey : John Wiley & Sons, Inc.

Stein, A. F., R. R. Draxler, G. D. Rolph, B. J. B. Stunder, M. D. Cohen, and F. Ngan (2015), NOAA's HYSPLIT Atmospheric Transport and Dispersion Modeling System, *Bulletin of the American Meteorological Society*, *96*(12), 2059-2077, doi:10.1175/bams-d-14-00110.1.

Stephens, G. L., T. L'Ecuyer, R. Forbes, A. Gettelmen, J.-C. Golaz, A. Bodas-Salcedo, K. Suzuki, P. Gabriel, and J. Haynes (2010), Dreary state of precipitation in global models, *Journal of Geophysical Research: Atmospheres*, *115*(D24), doi:10.1029/2010jd014532.

Twohy, C. H., et al. (2013), Impacts of aerosol particles on the microphysical and radiative properties of stratocumulus clouds over the southeast Pacific Ocean, *Atmospheric Chemistry and Physics*, *13*(5), 2541-2562, doi:10.5194/acp-13-2541-2013.

Twohy, C. H., et al. (2002), Deep convection as a source of new particles in the midlatitude upper troposphere, *Journal of Geophysical Research: Atmospheres*, *107*(D21), AAC 6-1-AAC 6-10, doi:10.1029/2001jd000323.

Twohy, C. H., et al. (2020 submitted), Cloud-Nucleating Particles over the Southern Ocean in a Changing Climate, *Atmospheric Chemistry & Physics Discussion*.

Twohy, C. H., A. J. Schanot, and W. A. Cooper (1997), Measurement of Condensed Water Content in Liquid and Ice Clouds Using an Airborne Counterflow Virtual Impactor, *Journal of Atmospheric and Oceanic Technology*, *14*(1), 197-202, doi:10.1175/1520-0426(1997)014<0197:Mocwci>2.0.Co;2.

Twomey, S. (1977), The Influence of Pollution on the Shortwave Albedo of Clouds, *Journal of the Atmospheric Sciences*, *34*(7), 1149-1152, doi:10.1175/1520-0469(1977)034<1149:Tiopot>2.0.Co;2.

Weber, R. J., G. Chen, D. D. Davis, R. L. Mauldin, D. J. Tanner, F. L. Eisele, A. D. Clarke, D. C. Thornton, and A. R. Bandy (2001), Measurements of enhanced H2SO4 and 3-4 nm particles near a frontal cloud during the First Aerosol Characterization Experiment (ACE 1), *Journal of Geophysical Research-Atmospheres*, *106*(D20), 24107-24117, doi:10.1029/2000jd000109.

Williams, K. D., A. Bodas-Salcedo, M. Déqué, S. Fermepin, B. Medeiros, M. Watanabe, C. Jakob, S. A. Klein, C. A. Senior, and D. L. Williamson (2013), The Transpose-AMIP II Experiment and Its Application to the Understanding of Southern Ocean Cloud Biases in Climate Models, *Journal of Climate*, *26*(10), 3258-3274, doi:10.1175/jcli-d-12-00429.1.

Williamson, C. J., et al. (2019), A large source of cloud condensation nuclei from new particle formation in the tropics, *Nature*, *574*(7778), 399-403, doi:10.1038/s41586-019-1638-9.

Wood, R., et al. (2018), Ultraclean Layers and Optically Thin Clouds in the Stratocumulus-to-Cumulus Transition. Part I: Observations, *Journal of the Atmospheric Sciences*, *75*(5), 1631-1652, doi:10.1175/jas-d-17-0213.1.

Yu, F., and G. Luo (2010), Oceanic Dimethyl Sulfide Emission and New Particle Formation around the Coast of Antarctica: A Modeling Study of Seasonal Variations and Comparison with Measurements, *Atmosphere*, *1*(1), 34-50, doi:10.3390/atmos1010034.

Zheng, G., et al. (2018), Marine boundary layer aerosol in the eastern North Atlantic: seasonal variations and key controlling processes, *Atmospheric Chemistry and Physics*, *18*(23), 17615-17635, doi:10.5194/acp-18-17615-2018.

Zhou, X., R. Atlas, I. L. McCoy, C. S. Bretherton, C. Bardeen, A. Gettelman, P. Lin, and Y. Ming (2020 submitted), Evaluation of cloud and precipitation simulations in CAM6 and AM4 using observations over the Southern Ocean, *Journal of Geophysical Research: Atmospheres*.